Universidade Federal do Rio de Janeiro

Centro de Ciências Matemáticas e da Natureza

Observatório do Valongo

Laboratório de Astrofísica Extragaláctica

Star Formation Quenching in Green Valley Galaxies at Intermediate Redshifts

Ph.D. Student: João Paulo Nogueira-Cavalcante

Advisor: Karín Menéndez-Delmestre

Co-Advisor: Thiago Signorini Gonçalves

Rio de Janeiro

Abril de 2017

Star Formation Quenching in Green Valley Galaxies

at Intermediate Redshifts

João Paulo Nogueira Cavalcante

Dra. Karín Menéndez-Delmestre (Orientadora)
Dr. Thiago Signorini Gonçalves (Coorientador)

Tese de doutorado submetida ao Programa de Pós-Graduação em Astronomia, Observatório do Valongo, da Universidade Federal do Rio de Janeiro - UFRJ, como parte dos requisitos necessários à obtenção do título de Doutor em Ciências - Astronomia.

Aprovada por:

Presidente, Dra. Karín Menéndez-Delmestre - (Orientadora) – OV/UFRJ

Dr. Thiago Signorini Gonçalves - (Coorientador) - OV/UFRJ

Dra. Paula Rodrigues Teixeira Coelho – (Avaliadora Externa) – IAG/USP

Dr. Marco Grossi – (Avaliador Externo) – ON/MCTIC

Dra. Aldée Marie Clémence Charbonnier– (Avaliadora Interna) – OV/UFRJ

Dr. Paulo Afrânio Augusto Lopes (Avaliador Interno) – OV/UFRJ

Rio de Janeiro
Abril de 2017

CIP - Catalogação na Publicação

NC376s
s

Nogueira Cavalcante, João Paulo
Star formation quenching in green valley galaxies ar intermediate redshifts / João Paulo Nogueira Cavalcante. -- Rio de Janeiro, 2017.
xviii, 76 f.

Orientadora: Karín Menéndez-Delmestre.
Coorientador: Thiago Signorini Gonçalves.
Tese (doutorado) - Universidade Federal do Rio de Janeiro, Observatório do Valongo, Programa de Pós Graduação em Astronomia, 2017.

1. Formação estelar. 2. Redshifts intermediários. 3. Vale verde. 4. Galáxias. I. Menéndez-Delmestre, Karín, orient. II. Signorini Gonçalves, Thiago, coorient. III. Título.

Elaborado pelo Sistema de Geração Automática da UFRJ com os dados fornecidos pelo(a) autor(a).

Este trabalho é dedicado às minhas filhas,
Maria Eduarda e Maria Clara.

One day in your life

You'll remember a place

Someone touching your face

You'll come back and

you'll look around, you'll ...

One day in your life

You'll remember the love you found here

You'll remember me somehow

Though you don't need me now

I will stay in your heart

And when things fall apart

You'll remember one day ...

One day in your life

When you find that you're always waiting

For a love we used to share

Just call my name, and I'll be there

You'll remember me somehow

Though you don't need me now

I will stay in your heart

And when things fall apart

You'll remember one day ...

One day in your life

When you find that you're always longing

For a love we used to share

Just call my name, and I'll be there

One day in your life

Michael Jackson

Acknowledgements

Agradeço à UFRJ, e em especial ao Observatório do Valongo, por me proporcionarem o aprendizado básico através de disciplinas cursadas no ínicio do Doutorado e por me cederem o espaço para a realização da minha pesquisa.

À CAPES pela ajuda financeira através de uma bolsa de Doutorado.

Aos meus sempre queridos orientadores, Karín Menéndez-Delmestre e Thiago S. Gonçalves, pelos esforços árduos que tiveram ao longo desses quatros anos para que esta tese fosse realizada. Jamais me esquecerei dos seus ensinamentos. Meus profundos e sinceros agradecimentos por terem me orientado de forma tão ativa e agradável.

À Aldeé Charbonnier, Laurie Riguccini e ao Kartik Sheth, pelas contribuições que foram, além de importantes, extremamente necessárias para a conclusão desta tese. Além de colaboradores se tornaram grandes amigos.

Aos meus colegas de sala Bruno Coelho, Raquel Nascimento, Hélio Perottoni e Elisson Saldanha. Foi ótimo o convívio que tivemos e espero poder encontrá-los novamente. Muito obrigado por terem compartilhado seu tempo comigo.

Aos meus amigos de infância Betinho e Fabiano por me considerarem um irmão e estarem sempre presentes nas horas que precisei. Sempre acharam que a minha profissão é coisa de maluco mas sempre me motivaram para continuar.

Aos meus colegas de comércio, Cleiton e Túlio, pelas vezes que seguraram o trampo no meu lugar e pelas boas conversas que sempre tivemos e também à Baixinha e à Vera pelas tantas vezes que cuidaram das minhas filhas por mim. Meus sinceros agradadecimentos a vocês.

Meus agradecimentos especiais à minha maravilhosa família. À minha mãe, Marilza, e ao meu pai, João Antônio, principais financiadores da minha educação e sempre importantes renovadores da minha esperança. Aos bons exemplos que me deram e ao grande incentivo que tive deles para continuar em frente e nunca desistir. Ao meu irmão, Thiago, pela preocupação e carinho que sempre teve por mim. Ao meu tio, Adalberto, pelo grande exemplo que deu sobre o valor que devemos dar aos frutos do trabalho. Amo todos vocês.

Um agradecimento todo especial vai à minha companheira Raquel pelo companheirismo, pela dedicação constante, pelos momentos de felicidades, pelos momentos difíceis, pelo amor que tem por mim. Pelas vezes que não deixou que eu desistisse do Doutorado. E principalmente, por ter me dado a Maria Eduarda e a Maria Clara. Sempre te amarei.

Finalmente, eu agradeço o meu querido povo brasileiro, que contribuiu à minha formação e estadia nesta Universidade. Estes últimos anos de recessão econômica foram bastante penosos para o meu país e espero sinceramente estar retribuindo o investimento que eu tive da minha querida pátria, Brasil.

Abstract

The color-magnitude diagram of galaxies reveals two distinct galaxy populations, one containing blue star-forming galaxies and the other dominated by red passive objects. Between these blue and red peaks there is a region known as the *green valley*, which can be considered as a transitional stage as galaxies go from gas-rich star-forming galaxies to gas-poor passive ones. Recent work has shown that galaxies quench their star formation and hence traverse the green valley 5 times faster at $z \sim 0.8$, when compared to the nearby universe, where the typical quenching timescale is ~ 1 Gyr. This indicates that the specific processes responsible for this transition at intermediate redshifts must be distinct from those that dominate the transition today. To probe this, in this thesis we calculate the star formation quenching timescales in green valley galaxies at $0.5 < z < 1.0$. To do this we use the optical spectra of galaxies and assume a star formation history with an exponential decline. We study the derived quenching timescales as a function of *morphological type*, *compactness* and the *presence of an active galactic nucleus* (AGN). We find that different galaxy morphologies (ellipticals, unbarred disks, weakly barred disks, strongly barred disks, irregulars and merging galaxies) present different star formation quenching timescales, reinforcing the idea that the galaxy morphology is strongly correlated with the physical processes responsible for quenching star formation. We find that disks have typical timescales 60% to 5 times longer than that of galaxies presenting spheroidal, irregular or merger morphologies. This suggests that disk galaxies are dominated by secular evolution (bar and spiral arms) whereas elliptical, irregular and merger systems are associated with processes which quench star formation faster, such as galaxy interactions and/or violent disk instabilities. Considering the compactness we find that the star formation quenching timescales in green valley compact and ultra-compact galaxies are $2 - 5$ times shorter than in normal-sized ones. These results are consistent with the violent disk instability scenario for the formation of compact galaxies, which is expected to rapidly quench star formation in such galaxies. Finally, we find that massive green valley galaxies with an AGN exhibit faster star formation quenching than their non-AGN counterparts, specially when galaxies residing in dense environments are removed. These

results suggest that although a mix in quenching mechanisms is present at intermediate redshifts, fast processes such as mergers, AGN and the environment may play a more important role in triggering the passage of galaxies through the green valley.

Resumo

O diagrama cor-magnitude de galáxias revela dois picos de populações, um contendo galáxias azuis que formam estrelas e o outro dominado por objetos vermelhos passivos. Entre esses picos azul e vermelho há uma região conhecida como *vale verde*, que pode ser considerado como um estágio transicional onde galáxias migram de sistemas ricos em gás que formam estrelas para sistemas pobres em gás cuja atividade de formação estelar é baixa ou nula. Trabalhos recentes mostraram que em $z \sim 0.8$ galáxias cessam sua formação estelar e assim atravessam o vale verde 5 vezes mais rápido que as do universo local, onde a escala de tempo de cessação da formação estelar típica é de ~ 1 bilhão de anos. Isto indica que os processos específicos responsáveis por esta transição em *redshifts* intermediários devem ser distintos que aqueles que dominam o universo local. Para investigar isso, nesta tese nós calculamos a escala de tempo da cessação da formação estelar em galáxias do vale verde em $0.5 < z < 1.0$. Para isto nós usamos espectros de galáxias no óptico e assumimos um histórico de formação estelar com uma queda exponencial. Nós estudamos essas escalas de tempo derivadas em função do *tipo morfológico*, *compacidade* e *precença de uma atividade de núcleo ativo* (AGN). Nós encontramos que diferentes morfologias (elípticas, discos sem barra, discos fracamente barrados, discos fortemente barrados, irregulares e galáxias em processo de fusão) apresentam diferentes escalas de tempo de cessação da formação estelar, reforçando a ideia que a morfologia das galáxias é fortemente correlacionada com os processos responsáveis em cessar a formação estelar. Nós encontramos que os discos têm escalas de tempo de cessação da formação estelar típicas de 60% a 5 vezes mais longas que a de galáxias elípticas, irregulares ou mesmo em processo de fusão. Isto sugere que galáxias discos são dominadas por evolução secular (barras e braços espirais) enquanto que galáxias elípticas, irregulares e sistemas em fusão são associadas com processos que cessam a formação estelar de forma rápida, tais como interações e/ou instabilidade violenta do disco. Considerando a compacidade nós encontramos que a escala de tempo de cessação da formação estelar em galáxias compactas e ultra-compactas do vale verde são $2 - 5$ vezes mais curta que em galáxias de tamanho normal. Estes resultados são consistentes com o cenário de instabilidade violenta do disco para a formação de

galáxias compactas, onde é esperado quem em tais galáxias a formação estelar cesse rapidamente. Finalmente, nós encontramos que galáxias do vale verde massivas com um AGN exibem rápida cessação da formação estelar em comparação com galáxias sem um AGN, especialmente quando removemos galáxias que residem em ambientes densos. Estes resultados sugerem que embora uma mistura de mecanismos que cessam a formação estelar está presente em *redshifts* intermediários, processos rápidos tais como fusão, AGN e processos ambientais são importantes na passagem de galáxias através do vale verde nestes *redshifts*.

Contents

List of Figures

List of Tables

Chapter 1

Introduction

Almost 100 years have gone by since the seminal work by Edwin Hubble in 1926, where he classified thousands of nebulae according to their apparent shape. His classification of extragalactic systems − separating them into ellipticals, barred and unbarred spirals, and irregulars (Figure 1.1) − is the reference for all morphological work that has been done since then. This classification system has been updated by several authors along the years (e.g., de Vaucouleurs, 1959; Kormendy & Bender, 1996; Sandage, 1961).

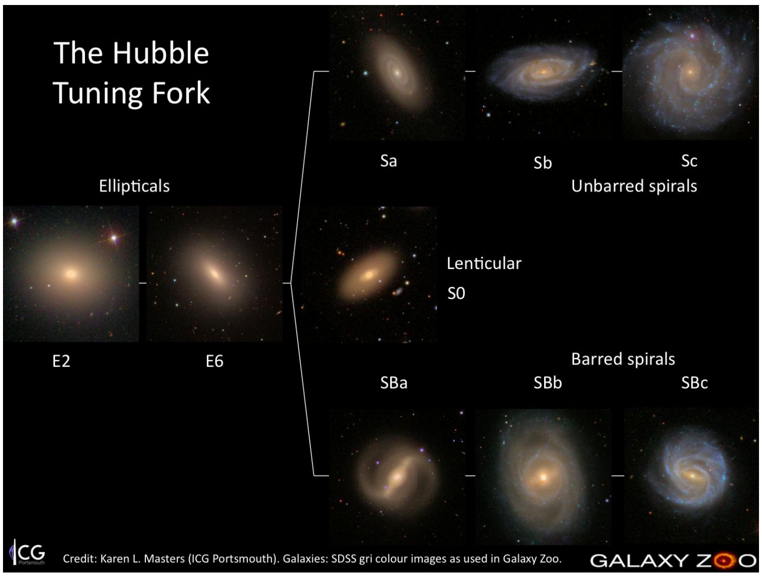

Figure 1.1: Hubble tuning fork diagram, separating galaxies in elliptical, lenticular and disk (barred and unbarred).

At the origin of this classification system, Hubble suggested an evolutionary connection for galaxies on the left side of the tunning-fork diagram (so-called "early-type galaxies") shown in Figure 1.1 towards the so-called "late-type galaxies" on the right side. Although the diagram is no longer associated to an a evolutionary sequence, the terms of early- and late-type galaxies remain today as a form of referring to elliptical and lenticular galaxies, and spirals and irregulars, respectively. A clear distinction in properties between early- and late-type galaxies has been well established over the years. Most strikingly, a difference in the overall color of these galaxies can be observed immediately from broad-band photometry; this is clear from Figure 1.1.

With the advent of large multi-band surveys using optical broad band photometry, it was possible to construct color-magnitude diagrams (CMD) of thousands to millions of galaxies, allowing for a more statistical analysis of this systematic difference in colors. In fact, a distinct color bimodality based on $u - r$ colors from the Sloan Digital Sky Survey (SDSS, Stoughton et al., 2002) was readily observed (Strateva et al., 2001; Baldry et al., 2004, 2006). The CMD of SDSS galaxies revealed a distinct peak in number density towards redder colors and a second one towards bluer colors. Subsequent studies (e.g., Kauffmann et al., 2003) have pointed out to differences in physical properties between galaxies in the two peaks, revealing that red peak galaxies (the so-called "red sequence" galaxies) typically have older stellar populations than those in the blue peak ("blue cloud" galaxies). With a marked extension towards brighter $r-$band magnitudes and considering that $r-$band is sensitive to the amount of stellar mass, these red sequence galaxies also appear to dominate the high-mass end.

When the Galaxy Evolution Explorer (GALEX; Martin et al., 2005) was launched in 2003, the all-sky availability of ultraviolet broad band photometry marked a new era: with a near-UV band, sensitive to the peak of young (< 100 Myrs) stars, GALEX became key for the study of young, star-forming systems. Taking advantage of this, Wyder et al. (2007) demonstrated that a CMD based on NUV$-r$ colors, combining GALEX and SDSS photometry, was significantly more effective at separating the blue cloud and red sequence populations. Furthermore, they showed that the CMD was not merely composed of two populations of galaxies with nothing in between; the blue and red peaks were not well fit by a double Gaussian function. At this time, the region between the blue cloud and the red sequence, merely noted as a rather empty-region between two peaks, acquired its own identity and the term "green valley" was coined (see Figure 1.2, Salim et al., 2007).

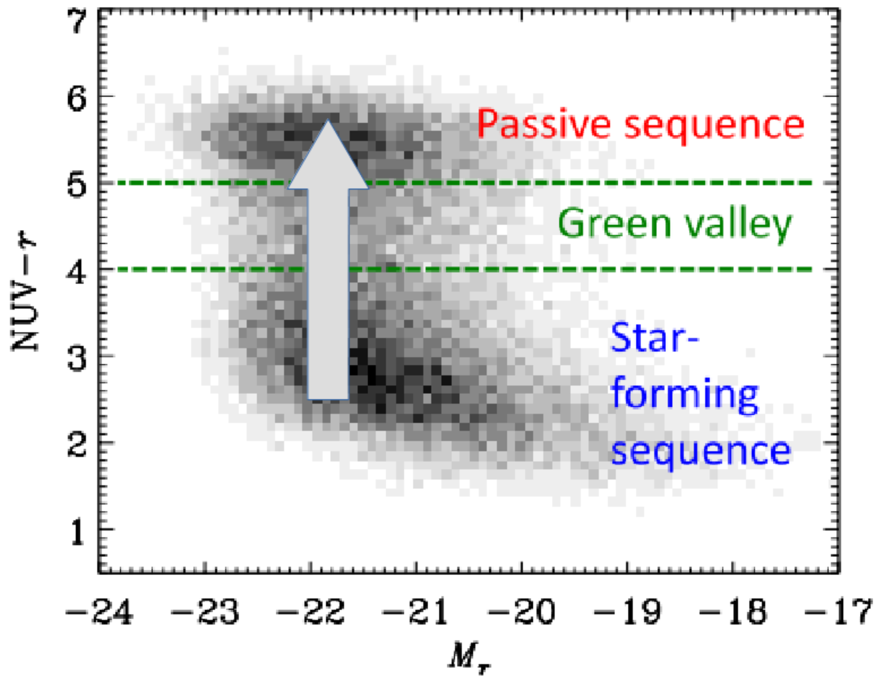

Figure 1.2: Color-magnitude diagram of the SDSS/GALEX galaxies at $z < 0.22$ (Salim et al., 2007), showing clearly the different galaxy populations (blue cloud, green valley and red sequence). The horizontal axis represents the SDSS r-band absolute magnitude and the vertical axis represents the NUV$-r$ color. The dashed horizontal lines delimit the green valley region. The gray arrow illustrates the passage of a galaxy on the CMD: from the blue cloud to the red sequence, passing through the green valley.

Many differences have been identified between galaxies in the blue cloud and those in the red sequence: blue cloud galaxies are typically gas-rich galaxies with predominantly young populations and active star formation, while red sequence galaxies are for the most part passive gas-poor galaxies with older stellar populations.

Moreover, Pan et al. (2013) have shown that stellar populations in green valley galaxies are older than those in blue cloud galaxies and younger than those in red sequence galaxies. This supports an evolutionary scenario on the galaxy CMD, where blue galaxies evolve into red ones, transitioning through the green valley. This points to the green valley as a transitional phase of galaxy evolution.

During the blue cloud phase, galaxies typically experience a period of steady-state of star formation activity, when the star formation rate (SFR) is directly proportional to the gas content (Schmidt, 1959; Kennicutt, 1998), so that more gas-rich galaxies form stars at a faster rate and galaxies with less gas use up their fuel at a slower pace. Furthermore, a typical star-forming galaxy will form stars at a rate congruent with its stellar mass − a reflection of the observed correlation between SFR and stellar mass for typical star-forming galaxies known as the "main sequence" of star-forming galaxies (Noeske et al., 2007). As we go out to higher redshifts, the star-forming main sequence is displaced towards higher SFRs and higher stellar masses, but the connection between these two proprieties is otherwise maintained out to $z \sim 2.5$ (Whitaker et al., 2012).

As a galaxy evolves out of the star formation main sequence (MS), galaxy colors change and the galaxy transition across the galaxy CMD begins, passing through the green valley, ultimately reaching the red sequence. The formation of stars is a mechanism that naturally uses up the gas available in a galaxy. In a steady-state situation, the duration of star formation would be proportional to the gas content and inversely proportional to the star formation rate; this corresponds to the depletion time, the time it takes for the galaxy to use up all of its available fuel with the current SFR.

The typical depletion timescale for main sequence star-forming galaxies in the local universe is ∼2 Gyrs (Bigiel et al., 2008), while at higher redshifts this is significantly shorter ($\sim$ 700 Myrs at $z = 3$, Tacconi et al., 2013). However, pure star formation activity cannot explain the observed growth of the red sequence as measured by Faber et al. (2007). These authors report that, although the massive end of the red sequence was already in place at least at $z = 1$, the red sequence has increased in number by approximately a factor of two since $z \sim 1$. This result suggests that the build-up of the red sequence is a process that is ongoing at intermediate redshifts. Other processes that are able to interrupt star formation must be acting in galaxies, accelerating the passage of galaxies through the green valley. These star formation quenching mechanisms are responsible for the observed bimodality in the galaxy CMD.

There are many astrophysical processes that can impact the color, composition, gas content and global shape of galaxies (Figure 1.3). They have been the subject of many studies and are well recognized to be agents that can either trigger star formation in galaxies (e.g., mergers, disk instabilities) − leading to an accelerated exhaustion of the gas content − or directly quench the star-forming activity by expelling or heating the necessary fuel for continued star formation (e.g., feedback from an active galactic nucleus). For instance, major mergers have been shown to lead to strong gas inflows that trigger galaxy-wide starbursts (Springel et al., 2005); they can further lead to the growth of bulges and ultimately change the overall galaxy morphology (Cheung et al., 2012; Springel et al., 2005).

Feedback from supernovae in low-mass galaxies and active galactic nuclei (AGN) in massive galaxies have also been proposed as important quenching agents by either expelling or heating the gas that would otherwise collapse and form stars. In the case of massive galaxies, Nandra et al. (2007) studied a sample of X-rays sources and found that the majority of host galaxies are red, suggesting a scenario where the AGNs either cause or maintain the star formation quenching. Schawinski et al. (2009) reached a similar conclusion, finding that the majority of red sequence galaxies and those in the green valley host AGNs. In the case of low-mass galaxies, supernovae winds have been shown to be capable of quenching star formation, expelling the gas from the interstellar medium (Lagos et al., 2013).

Internal secular processes including disk instabilities (e.g., bars) have been associated with significant gas inflow responsible for the rapid consumption of gas through nuclear starbursts and the formation of pseudobulges (Ho et al., 1997; Kormendy & Kennicutt, 2004; Sheth et al., 2005). External secular processes driven by the environment, such as strangulation, ram-pressure stripping and harassment, have also been shown to remove or heat gas in galaxies as they enter high-density regions (Coil et al., 2008; Dekel et al., 2003; Farouki & Shapiro, 1981; Gunn & Gott, 1972; Larson et al., 1980; Mendez et al., 2011; Moore et al., 1998), thus contributing to stop star formation in these systems.

Many of these processes have been studied in their roles as quenching agents, but their relative contributions towards quenching the general galaxy population still remains an open question, both locally and at higher redshifts. A brief review

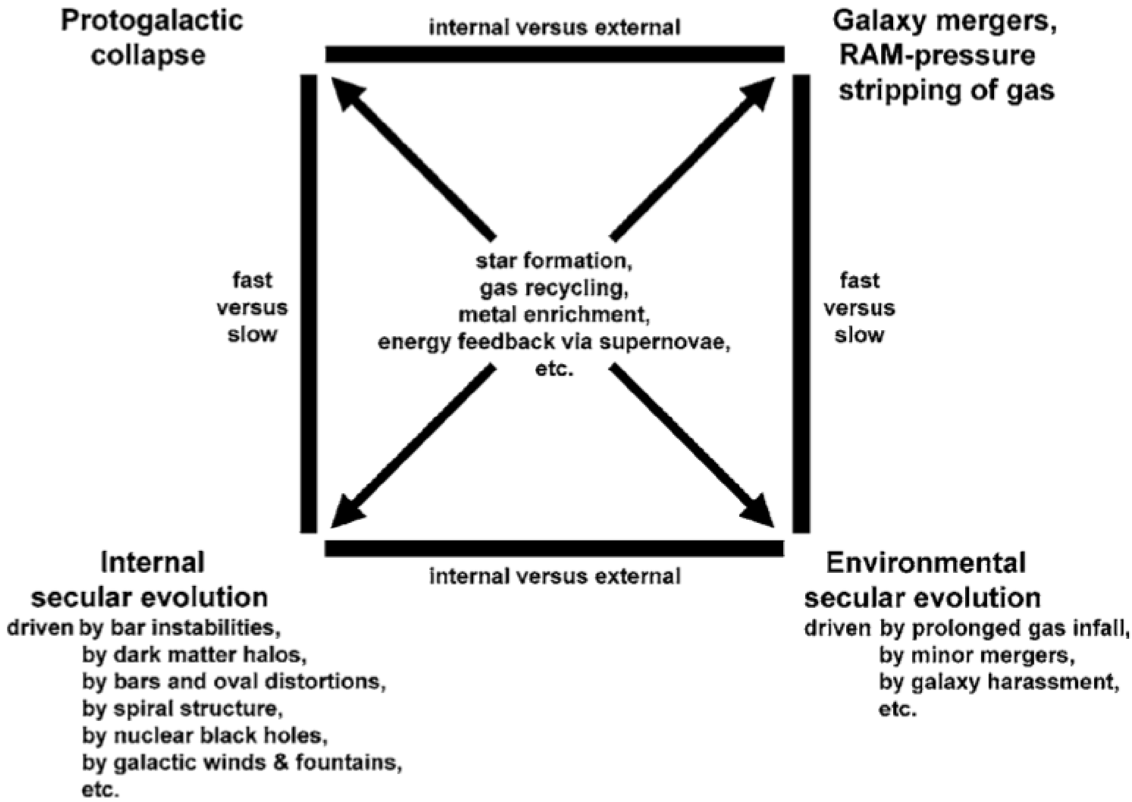

Figure 1.3: A summary of the physical mechanisms at play as galaxies evolve (taken from Kormendy & Kennicutt, 2004). The processes are divided vertically into *fast* ones, which can take some hundreds of millions years (top) and *slow* ones, which can take a few billion years (bottom). Horizontally the processes are divided into *internal* (left) and *external* (right). At the center of the square are the processes which happen typically in all galaxies and can be affected by the processes outside the square.

of the main results that have been collected over the last decade shows how much controversy exists in the field.

Peng et al. (2010) suggested that fast processes (e.g., major mergers) play a very important role in the evolution of galaxies at early times ($z \sim 1-2$). However, Mendez et al. (2011), using quantitative morphological parameters, found that although mergers are common at $0.4 < z < 1.2$ their fraction within the green valley is lower than that in the blue cloud, suggesting that mergers are not important for quenching star formation in green valley galaxies at these redshifts.

At later times ($z \sim 0$), mergers become less common (Conselice et al., 2003), and slower processes that generally involve interactions between stars, gas clouds and the dark matter halo (e.g., disk instabilities, bars) may become more important (Spitzer & Schwarzschild, 1951, 1953). However, Martin et al. (2007) found that $\sim 50\%$ of green valley galaxies at $z \sim 0.1$ show signs of AGN activity, although the AGN luminosity was not found to be correlated with the timescale of star formation quenching. Considering that AGN activity is usually associated with fast star formation quenching, as demonstrated by hydrodynamical simulations (Dubois et al., 2013; Sijacki & Springel, 2006), faster processes may also play an important role in quenching star formation at lower redshifts.

The role of the environment in quenching star formation across cosmic times is also not well establish. Kauffmann et al. (2003) have shown that the environment mechanisms are effective only in scales smaller than < 1 Mpc. This is at odds Balogh et al. (2004), who showed that the specific star formation rate (sSFR=SFR/$M_\star$) is a function of environment in scales greater than 1 Mpc. More recently, Pan et al. (2013) analyzed the environments of ~ 2000 green valley galaxies and found that at $z > 0.7$ they reside in environments of similar number density as those of blue galaxies. However, Darvish et al. (2016) reported that environment has likely had an impact on star formation quenching already since $z \sim 1$ and, therefore, the environment in green valley galaxies should be different from that of blue cloud galaxies at $z < 1$.

Although much debate exists on the role of merger, AGNs and secular evolution as main drivers of galaxy transition through the green valley either at low or high redshifts, recent work by Martin et al. (2007) and Gonçalves et al. (2012) have shown that the galaxy transition through the green valley varies with cosmic time. Through the quantification of the star formation quenching timescales together with measurements of stellar masses and galaxy number densities on the CMD, Martin et al. (2007) and Gonçalves et al. (2012) measured the mass flux through the green valley and concluded that the galaxy transition through the green valley is 5 times faster at $z \sim 0.8$ than at $z \sim 0.1$. Moreover, these studies showed that more massive systems are transiting the green valley in the distant universe. With such a galaxy flow through the green valley, Gonçalves et al. (2012) demonstrated a match with the buildup of the red sequence (Faber et al., 2007) at a time prior to the establishment of the Hubble sequence observed today (Delgado-Serrano et al., 2010).

In this thesis we quantify typical star formation quenching timescales for green valley galaxies at intermediate redshifts ($0.5 < z < 1.0$) as a function of galaxy morphology, compactness and the presence of an AGN. Focusing on green valley galaxies at similar redshifts to those studied by Gonçalves et al. (2012), we aim to elucidate on the reasons why the green valley phase is significantly shorter at these redshifts, when compared to that at lower redshifts. We expand beyond the work of Gonçalves et al. (2012) by focusing on the specific physical mechanisms responsible for the quenching of star formation in green valley galaxies at these redshifts. Considering the transitional nature of the green valley phase, at intermediate redshifts we are studying the progenitors of red passive galaxies in the local universe. Having a clear picture of the astrophysical processes that dominate the quenching of the intermediate-redshift green valley galaxies is thus critical to our understanding of the formation of red sequence galaxies, in particular at intermediate-to-low masses were the bulk of the red sequence has grown at $z < 1$.

This Ph.D. thesis is organized as follows. In Chapter 2 we present the methodology used to measure the star formation quenching timescales and the photometric and spectroscopic data used for the analysis in this thesis. In Chapters 3, 4 and 5 we show our analysis on the star formation quenching as a function of galaxy morphology, compactness and the presence of AGN. Finally, in Chapter 6 we summarize our findings and present our main conclusions on galaxy transition through the green valley at $0.5 < z < 1.0$. We use standard cosmology throughout this Ph.D. thesis, with $\Omega_M = 0.3$, $\Omega_\Lambda = 0.7$ and $h = 0.7$.

Chapter 2

Determination of Star Formation Quenching Timescales of Green Valley Galaxies in the COSMOS Field

Estimating the time it takes for a galaxy to traverse the green valley as it quenches its star formation and becomes a red passive system is at the core of our analysis. Based on optical spectra of green valley galaxies and assuming a simple model of star formation history with an exponential decay, we study two spectral indices − the rest-frame 4000 Å break and the equivalent width of the H_δ − that are very sensitive to the age of the stellar population and to different star formation histories (Kauffmann et al., 2003). This approach has been successfully used by Martin et al. (2007) on low-redshift ($z \sim 0.1$) SDSS galaxies and by Gonçalves et al. (2012) at higher redshifts ($z \sim 0.8$). We describe it in detail in this Chapter, applied to our sample of green valley galaxies identified within the COSMOS field.

2.1 Methodology

To quantify star formation quenching timescales, we adopt the approach used by Martin et al. (2007) and Gonçalves et al. (2012). We make a simplifying assumption on the star formation history (SFH) for each galaxy, where the star formation rate (SFR) is parameterized in the following way:

$$\mathrm{SFR}(t) = \mathrm{SFR}(t = 0), \quad t < t_0; \tag{2.1}$$

$$\mathrm{SFR}(t) = \mathrm{SFR}(t = 0)e^{-\gamma t}, \quad t > t_0 \ , \tag{2.2}$$

where t_0 is a characteristic time. Equations 2.1 and 2.2 tell us that the SFH for each galaxy can be described by a constant SFR until $t = t_0$, followed by a period of exponential decay. The γ index, in units of Gyr^{-1}, characterizes the "rate" at which star formation is quenched and is the quantity that we aim to measure. A smaller γ value corresponds to slower quenching, whereas a larger one corresponds to faster quenching. Within this simple model of SFH, the time evolution of the SFR strongly depends on the value of γ (see top panel in Figure 2.1): higher γ values translate into increasingly more abrupt drops in SFR at $t > t_0$. Since our focus is precisely on how fast green valley galaxies are experiencing this drop in SFR, our methodology is not dependent on the exact value of t_0. Considering that our analysis is directed towards galaxies with redshifts $z \sim 0.8$ that are within the green valley (and thus, experiencing already this drop in SFR), we choose for convenience t_0 to be equal to the age of the universe at $z = 0.8$. Therefore our SFH model assumes a constant SFR for the first $t_0 = 6$ Gyrs, followed by a period of exponential decay. This is the same approach adopted by Gonçalves et al. (2012) in his work on $z \sim 0.8$ green valley galaxies.

The exponential index γ can be obtained by applying the methodology described in Kauffmann et al. (2003), based on measuring the rest-frame 4000 Å break and the strength of the H_δ absorption line. The 4000 Å break corresponds to a discontinuity in the optical spectrum of a galaxy caused mainly by the opacity in the metal-rich stellar atmospheres: in a galaxy dominated by young stellar populations, the 4000 Å break will be small because the metals in the atmospheres of O and B stars that dominate the galaxy's optical spectrum are multiply-ionized and the ultraviolet radiation is not absorbed. The 4000 Å break becomes larger with older stellar populations. We quantify the 4000 Å break with the index defined in Balogh et al. (1999):

$$\mathrm{D}_n(4000) = \sum_{\lambda=4000\text{Å}}^{4100\text{Å}} F_\lambda \Bigg/ \sum_{\lambda=3850\text{Å}}^{3950\text{Å}} F_\lambda \ , \tag{2.3}$$

where F_λ is the flux at wavelength λ.

The H_δ absorption is strongest for galaxies that experienced a star formation burst in the past $0.1 - 1$ Gyr ago, once O and B stars have finished their evolution, and the stellar light is dominated by A stars. The $H_{\delta,A}$ index follows the same definition as Gonçalves et al. (2012), introduced by Worthey & Ottaviani (1997):

$$\mathrm{H}_{\delta,A} = \sum_{\lambda=4083{,}5\text{Å}}^{4122{,}25\text{Å}} \left(1 - \frac{F_\lambda}{F_{\lambda,\mathrm{cont}}}\right) d\lambda \ , \tag{2.4}$$

where $F_{\lambda,\mathrm{cont}}$ is the continuum flux. We define the continuum flux by fitting a straight line through the average flux density between 4041.60 Å and 4079.75 Å, bluewards of the H_δ absorption feature, and 4128.50 Å and 4161.00 Å, redwards.

The $H_{\delta,A}$ and $D_n(4000)$ indices have been shown to be sensitive to the galaxy SFH (Kauffmann et al., 2003). Both indices, as well as the global optical colors, are observables that depend strongly on the SFH of each galaxy. Figure 2.1 shows the time variation of the $H_{\delta,A}$ and $D_n(4000)$ spectral indices, as well as that of the NUV$-r$ color, for SFHs with different star formation quenching indices (γ).

Based on synthetic spectra we create a grid of curves in the $H_{\delta,A}\times D_n(4000)$ plane, each representing a model galaxy with a distinct star formation quenching index (see Figure 2.2). Along each curve, we identify the $H_{\delta,A}$ and $D_n(4000)$ values for green valley galaxies of a given NUV$-r$ color. Figure 2.2 shows how the $H_{\delta,A}$ and $D_n(4000)$ indices can assume different values for galaxies with the same SFH models but different colors. These galaxy models were produced using the Bruzual & Charlot (2003) code, with Chabrier (2003) initial mass functions, Padova 1994 stellar evolutionary tracks and solar metallicity (Alongi et al., 1993; Bressan et al., 1993; Fagotto et al., 1994a,b).

We note that although the assumed SFH model of a constant SFR followed by a period of exponential decay is somewhat simplistic, several studies support that an exponential decay in star formation activity is a good approximation at $z < 1$ (e.g., Baldry et al., 2008; Behroozi et al., 2013). Moreover, the quenching index (γ) measured in this work is not sensitive to the SFH before the green valley phase and, therefore, the assumption of a constant star formation before the quenching phase bears no impact on our results.

Gonçalves et al. (2012) used the same methodology to measure the mass flux through the green valley – the quantity of mass per unit of time and volume traversing the green valley from the blue cloud to the red sequence – at $z \sim 0.8$. They find an agreement between their results and the buildup of the red sequence (Faber et al., 2007). These results exemplify the reliability of the methodology and furthermore provide a comparison sample of quenching indices at redshifts similar to our study.

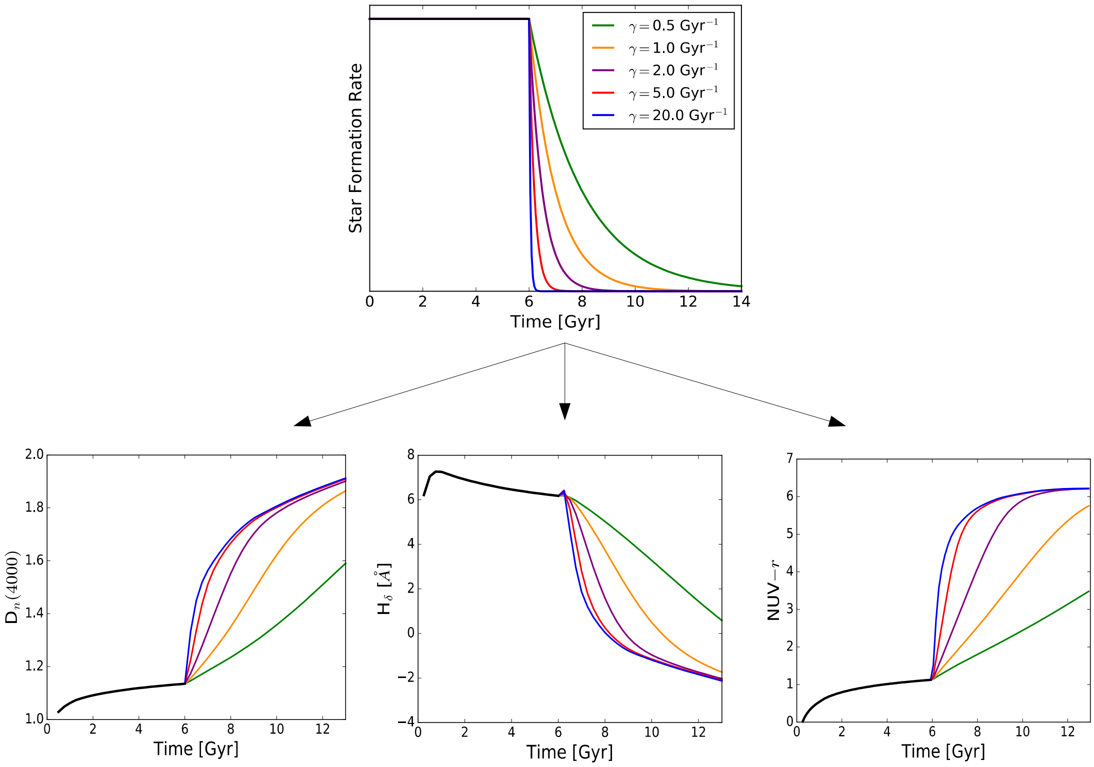

Figure 2.1: ***Top***: Star formation rate as a function of time for exponentially-decaying SFHs with five increasingly-steep decays given by increasingly-high γ indices (see Equations 2.1 and 2.2). ***Bottom***: $D_n(4000)$ and $H_{\delta,A}$ indices and NUV$-r$ color as functions of time, assuming the exponentially-decaying SFHs with different γ indices shown on the top panel. The faster the star formation quenching (i.e., higher γ value) is, the steeper the time variation of these indices will be.

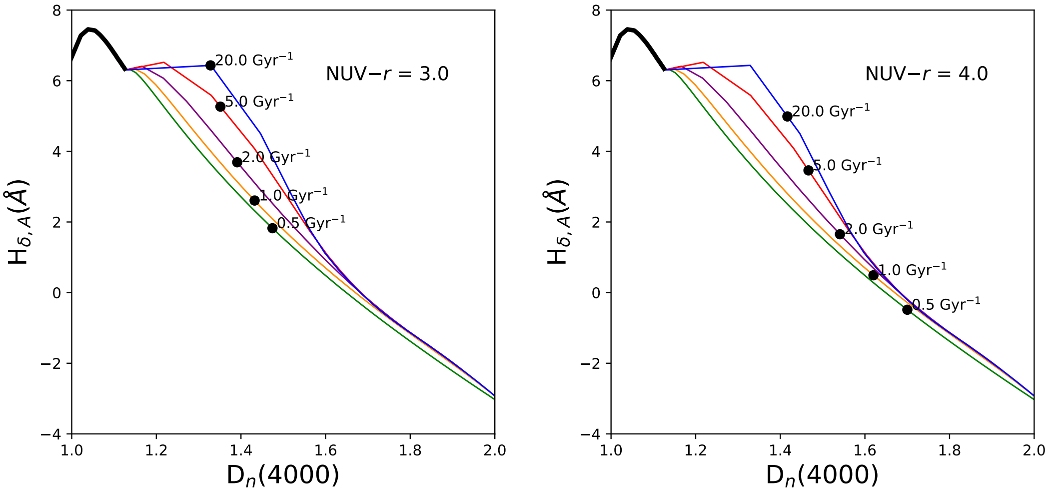

Figure 2.2: $H_{\delta,A} \times D_n(4000)$ planes for the five SFH models shown in Figure 2.1. The black dots represent the $H_{\delta,A}$ and $D_n(4000)$ values for a given SFH model and NUV$-r$ color. We can see clearly that different NUV$-r$ colors lead to different $H_{\delta,A}$ and $D_n(4000)$ values in the same SFH models.

2.2 Dataset - COSMOS Field

In this thesis we use COSMOS data to estimate the star formation quenching timescales in green valley galaxies and to link these timescales to the mechanisms responsible for the passage through the green valley at $0.5 < z < 1.0$. The COSMOS survey (Scoville et al., 2007) provides a very large combined dataset including:

- *multi-band photometry*, covering from the X-ray, ultraviolet (UV), optical, infrared, millimeter, to radio bands (e.g., Bertoldi et al., 2007; Capak et al., 2007; Hasinger et al., 2007; Sanders et al., 2007; Zamojski et al., 2007);
- *spectroscopic surveys*, including the zCOSMOS survey (Lilly et al., 2007) and the LEGA-C survey (van der Wel et al., 2016)

The collection of these datasets make COSMOS a valuable resource to define a large sample of high-redshift green valley galaxies based on photometry and to estimate their star formation quenching timescales based on available spectroscopy. We describe these details in the following sections.

2.2.1 Photometric Sample: the Canada-France-Hawaii Telescope Legacy Survey

To define a green valley sample, we first need to consider global galaxy colors. We determine NUV$-r$ rest-frame colors using photometry from the Canada-France-Hawaii Telescope Legacy Survey (CFHTLS), following the same procedure as in Gonçalves et al. (2012). We select galaxies with detections in all five CFHTLS bands (u,g,r,i,z), a necessary condition to correctly calculate the NUV and r rest-frame magnitudes for galaxies within the redshift range of $z \sim 0.5 - 1.0$, in order to properly separate the galaxy populations on the color-magnitude diagram for galaxies at our redshifts of interest. Considering that red galaxies are very faint in the rest frame NUV (traced by the u and g bands at $0.5 < z < 1.0$), this approach disfavors the selection of red sequence objects. However, this does not affect the completeness of the green valley and blue cloud galaxies because, by definition, these objects are relatively bright in the rest frame NUV. The rest-frame magnitudes were calculated using the *K-correct* code (version 4.2; Blanton & Roweis, 2007).

An important issue that must be taken into account in determining intrinsic galaxy colors is the contamination caused by dust, particularly in star-forming galaxies. We use the extinction correction model from Salim et al. (2009): they compare stellar population models attenuated by dust with observed spectral energy distributions to derive galaxy properties, including the SFR. They find the following relation:

$$A_{\mathrm{FUV}} = 3.68(\mathrm{FUV} - \mathrm{NUV}) + 0.29 \ , \tag{2.5}$$

where NUV and FUV are the rest-frame absolute magnitudes. To determine the extinction correction in other filters they use

$$A_\lambda \propto \lambda^{-0.7} \ . \tag{2.6}$$

We note that this procedure works well for dusty star-forming galaxies, but over-corrects the colors of dust-poor galaxies (Salim et al., 2009). Figure 2.3 shows the color-magnitude diagram of the CFHTLS galaxies with and without correction for dust extinction. We define our green valley galaxy sample by selecting objects with $2.0 <$ NUV$-r < 3.5$ in the dust-corrected CMD in an effort to mitigate the contamination of the green valley by dusty star-forming galaxies. Once we have minimized the presence of dusty star-forming galaxies from the green valley, we make the reasonable assumption that the observed colors of the green valley galaxy sample are effectively unaltered by dust. For this reason, we use the observed colors for the rest of the analysis.

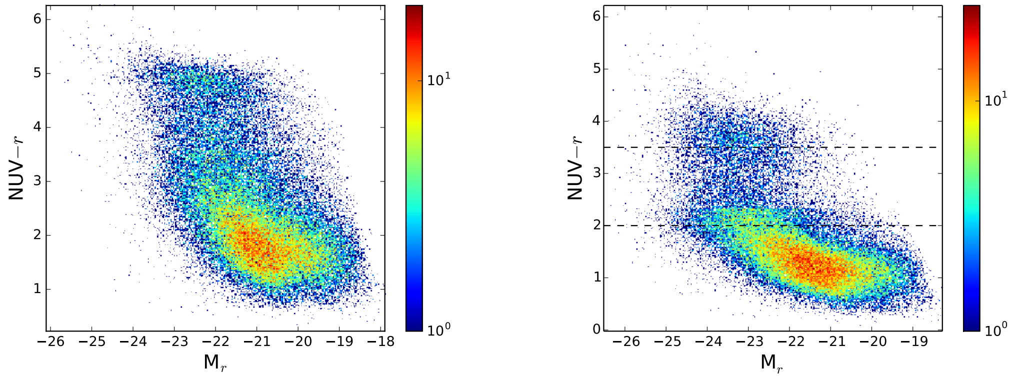

Figure 2.3: Color-magnitude diagrams of the Canada-France-Hawaii Telescope Legacy Survey galaxies used in this work. The left panel does not take into account the dust effects whereas the right panel is corrected by dust extinction. The horizontal axis represents the Sloan Digital Sky Survey r-band absolute magnitude and the vertical axis represents the color NUV$-r$ which can best distinguish the galaxy populations (blue cloud, green valley and red sequence). The dashed horizontal lines delimit the green valley region. The red sequence is not well represented because a requirement of this work is that all galaxies must be detected in all five CFHTLS photometric bands and the red galaxies are faint in the bluer bands.

2.2.2 Spectroscopic Sample: the zCOSMOS Survey

We exploit the zCOSMOS spectroscopic survey (Lilly et al., 2007) to obtain spectra for our green valley galaxies and measure the $D_n(4000)$ and $H_{\delta,A}$ spectral indices. This survey comprises ∼10,000 spectra (DR2) and ∼20,000 spectra (DR3) of galaxies in the COSMOS field with magnitudes down to $i = 22.5$, taken with the VIsible Multi-Object Spectrograph (VIMOS) located on the ESO Very Large Telescope (VLT). The spectral coverage of these spectra is from 5500Å to 9700Å, with a resolution of $R \sim 600$. This spectral coverage is ideal to measure the H_δ and $D_n(4000)$ indices within our redshift range of interest ($z \sim 0.5 - 1$).

2.3 Estimating the Quenching Timescales

The signal-to-noise ratio (S/N) of individual zCOSMOS spectra is too low to calculate the $D_n(4000)$ and, specially, the $H_{\delta,A}$ spectral indices with reasonable uncertainties to distinguish between different SFHs. The left panel of the Figure 2.4 shows the distribution of apparent magnitude in r-band from CFHTLS photometry of the green valley galaxies which have zCOSMOS spectra. Taking into account the last significant bin ($m_r \sim 24$), zCOSMOS integration time ~ 1 hr (Lilly et al., 2007) and an average redshift of ~ 0.8, the S/N around the H_δ absorption line is about one[1] (right panel of the Figure 2.4). The S/N required for this work around H_δ is ~ 4 (see Appendix A).

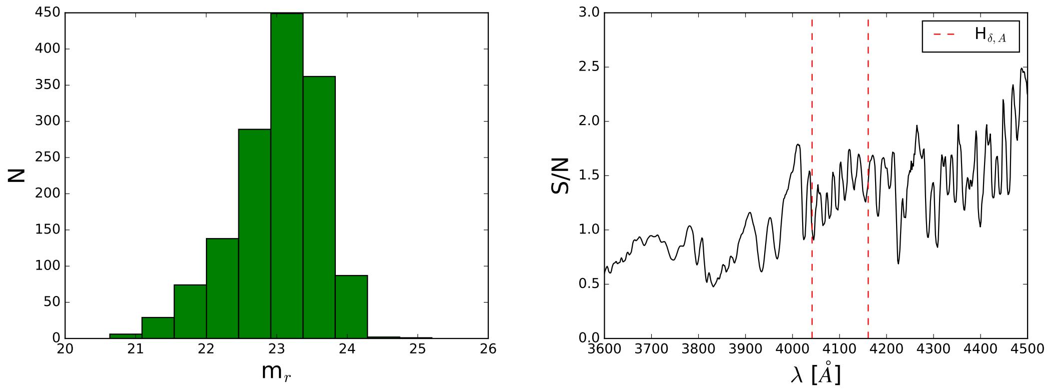

Figure 2.4: ***Left:*** Distribution of the apparent magnitudes in r-band (CFHTLS) of the zCOSMOS green valley galaxies from our sample. ***Right:*** Signal-to-noise as a function of wavelength for a faint point source ($m_r = 24$). The red vertical dashed lines delimit the H_δ absorption on the galaxy spectrum.

In order to increase the S/N and properly calculate the spectral indices we must coadd (stack) the zCOSMOS spectra. The procedure that we adopted for coadding galaxy spectra consist of calculating an initial median flux for each wavelength interval, identifying individual flux values beyond 2σ of the resulting distribution and rejecting these to calculate a new median; the process is repeated until the rejected entries reach a given pre-determined percentage of the population, which

[1]We estimated this value through the exposure time calculator, provided by the European Southern Observatory (https://www.eso.org/observing/etc/)

we set to 2% after confirming that varying this value had no impact on the resulting coadded spectra.

From a zCOSMOS galaxy coadded spectrum with sufficient S/N, we can measure $H_{\delta,A}$ and $D_n(4000)$ spectral indices. Based on these values, and considering the median NUV$-r$ color for the set of galaxies that make up the coadd we calculate the empirical star formation quenching index, γ, using the SFH model discussed in Section 2.1.

We note that model spectra from Bruzual & Charlot (2003) have a higher spectral resolution (R$\sim$ 3000) than the zCOSMOS spectra (R$\sim$ 600). In order to make our results robust, we created the grid of $H_{\delta,A}$ vs. $D_n(4000)$ model curves for different star formation quenching indices based on Bruzual & Charlot (2003) spectra degraded down to the same resolution as zCOSMOS spectra. The left panel of the Figure 2.5 shows an example of galaxy spectrum coadd.

For each coadd, we calculate the $H_{\delta,A}$ and $D_n(4000)$ indices and place them in the $H_{\delta,A}\times$ $D_n(4000)$ diagram (see right panel in Figure 2.5). We then consider the proximity of the coadd datapoint to the "green valley" position along the model curves corresponding to different γ values (black points on each of the colored curves in Figure 2.5). In order to more adequately interpolate between the different SFH models, we show the geometric average between two consecutive models with straight lines; for the didactic example shown in Figure 2.5, we identify the region associated to each γ value with a different color. The position of the measured $H_{\delta,A}$ and $D_n(4000)$ with respect to these lines enables us to determine which SFH model is a better fit to the data and hence associate a star formation quenching index, γ to the galaxy spectrum. Considering that each measured spectral index has its own error ($D_n(4000) \pm \sigma_{D_n(4000)}$ and $H_{\delta,A} \pm \sigma_{H_{\delta,A}}$), we generate a distribution of γ values for each coadd reflecting the spectral indices with their respective errors. For each coadd, the final value adopted for the quenching index corresponds to the average value of this distribution with an error corresponding to the standard deviation.

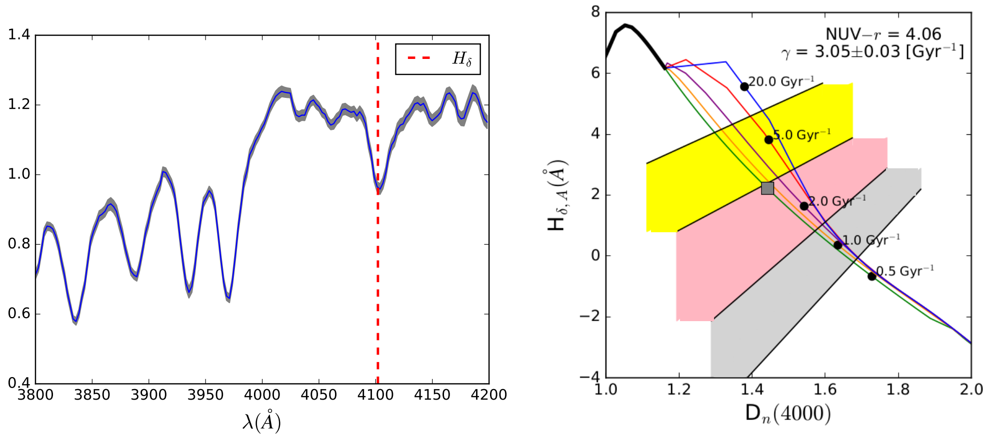

Figure 2.5: ***Left:*** Example of a spectrum resulting from the coadd of 100 randomly-selected zCOSMOS green valley spectra. The red dashed line highlights the wavelength position of the H_δ absorption line. ***Right:*** Similarly to Figure 2.2, $H_{\delta,A} \times D_n(4000)$ diagram with model curves for the five SFHs considered in our analysis, based on different star formation quenching indices ($\gamma = 0.5, 1.0, 2.0, 5.0, 20.0$ Gyr^{-1}). The black dots represent the "green valley" location associated to a specific NUV$-r$ color; in this case NUV$-r = 4.06$ is selected, as it corresponds to the median color of the $\sim$ 300 green valley galaxies whose zCOSMOS spectra comprise the coadd shown on the left panel. The gray square represents the value of $H_{\delta,A}$ and $D_n(4000)$ measured from the coadded spectrum. In this case, considering the high S/N of the spectrum, the error bars are not visible because the size of the square is larger. The value of the star formation quenching index (γ) associated to the coadd in question is $\gamma = 3.05 \pm 0.03$ Gyr^{-1}, corresponding to a star formation quenching timescale ($1/\gamma$) of 328 ± 3.2 Myrs.

Chapter 3

Star Formation Quenching as a Function of Morphology

For almost a century it has been known that massive galaxies ($> 10^{10.5}$ $M_\odot$) can be divided into two major morphological types: so-called early-type galaxies that include ellipticals and lenticulars; and late-types that include both barred and unbarred spirals (see Figure 1.1, Hubble, 1926). Galaxy morphologies are strongly correlated with other global properties, including color, star formation activity, gas content, environment and internal stellar dynamics. Elliptical galaxies, for instance, are typically red gas-poor systems with little star formation activity, residing preferentially in high-density cluster environments and are mainly supported by random motions of stars. On the other hand, spiral galaxies are typically blue gas-rich star-forming systems with stellar dynamics mainly supported by rotation on a disk.

The global morphology of a galaxy is also strongly correlated with its star formation history. Galaxies where star formation ceased Gyrs ago (e.g., red and dead massive ellipticals) tend to look very different from those where star formation continues at the present time (e.g., spiral and irregular galaxies). Furthermore, the many agents that alter the evolution of a galaxy (e.g., bars and mergers) may have a direct impact on the global shape of the system by redistributing stars within the galaxy.

Within the specific context of green valley galaxies, where galaxies are in the process of quenching their star formation, the different agents that quench star formation in galaxies leave morphological signatures in their host galaxies. This allows us to use galaxy morphology as a proxy for the astrophysical processes that may lead to star formation quenching.

In this Chapter we present our analysis on star formation quenching timescales as a function of galaxy morphology, considering that galaxy morphology provides us with an insight to the underlying galactic-scale transformations taking place.

3.1 Galaxy Morphology Classification

We base our morphological classifications on the Zurich Estimator of Structure Types (ZEST) catalog (Scarlata et al., 2007). This catalog classifies galaxies down to $i = 24$ in the COSMOS field according to morphology based on a principal component analysis (PCA) of the galaxy structure. We base ourselves on this catalog to separate galaxies in our sample into the following morphological classes: elliptical galaxies ($T_{ZEST} = 1$), disk galaxies ($T_{ZEST} = 2$) and irregular galaxies ($T_{ZEST} = 3$). We note that the distribution of ZEST morphological classifications within all green valley galaxies down to $i = 22.5$ (i.e., within the zCOSMOS spectroscopic sample) is dominated by ellipticals (∼51%), with significant contributions from disks (∼33%) and irregular galaxies (∼16%).

Scarlata et al. (2007) tested the ZEST morphologies using visual classifications for a $z = 0$ sample and found that the ZEST classification agrees well with published morphologies. However, this classification has its limitations at higher redshifts due to decreased spatial resolution that turns the parametric analysis of structural details increasingly challenging. For this reason we carefully inspected HST optical images (F814W, I band) for all green valley galaxies within the zCOSMOS sample and excluded from our sample the galaxies corresponding to the following cases: ZEST-classified ellipticals with evident tidal- or disk-like structures, ZEST-classified disks displaying multiple clumps reminiscent of coalesced mergers and ZEST-classified irregulars where a clear separation between galaxy pairs (or multiple companions) was taken as evidence of an early-stage merger. Considering that we refrained from re-classifying these galaxies into a different morphological type and rather opted for discarding them from our sample, this resulted in a sample reduction of 56%, 30% and 40% for the elliptical, disk and irregular galaxy classes, respectively. Although we reduced the galaxy sample analyzed by ∼50%, with this approach we ensure a higher degree of purity within the morphological classes in our analysis. The resulting distribution of morphologies within the green valley sample corresponds to 36% ellipticals, 40% disks and 16% irregulars.

Within the disk galaxy classification, we also identify galaxies containing weak or strong bars, based on the classification by Sheth et al. (2008). These authors identified 796 barred disks from a sample of ~ 2000 galaxies. Their bar classification was obtained using two independent methods: by visual inspection and through the ellipse-fitting technique, which is based on inspection of the ellipticity and position angle profiles that result from fitting elliptical isophotes to the 2D light distribution of disk galaxies (Menéndez-Delmestre et al., 2007). Our resulting classification for disk galaxies is hence that of strongly barred, weakly barred and unbarred galaxies. If a galaxy presents a bar, it would be consider as strongly barred if the ellipticity of the fitted isophote is > 0.65. Otherwise the galaxy is considered as weakly barred.

For our analysis we also added the *merging* galaxy type, which comprises clear examples of (major) mergers. We identified these based on visual inspection, identifying the presence of tidal tails pointing to interactions between multiple galaxies. The galaxy images for all the morphological types are shown in Figure 3.1.

3.2 Results

For each galaxy morphological type (disks, ellipticals, irregulars and merging galaxies) and the subgroups of disks (strongly barred, weakly barred and unbarred disk galaxies) we combine the green valley galaxy spectra and produce a coadded spectrum. The resulting green valley coadded spectra for the different morphological types are shown in Figure 3.2. Figure 3.3 shows the position of the $\mathrm{H}_{\delta,A}$ and $\mathrm{D}_n(4000)$ spectral indices measured for each of the coadded spectra shown in Figure 3.2. For each morphological type considered in our analysis, we show in Table 3.1 the number of galaxies that went into building each coadd, their average NUV$-r$ color, as well as the resulting star formation quenching index (γ) and corresponding error (σ_γ).

Our results are summarized in Figure 3.4. We find that disk galaxies have the longest star formation quenching timescales ($\gtrsim$250 Myrs), while green valley

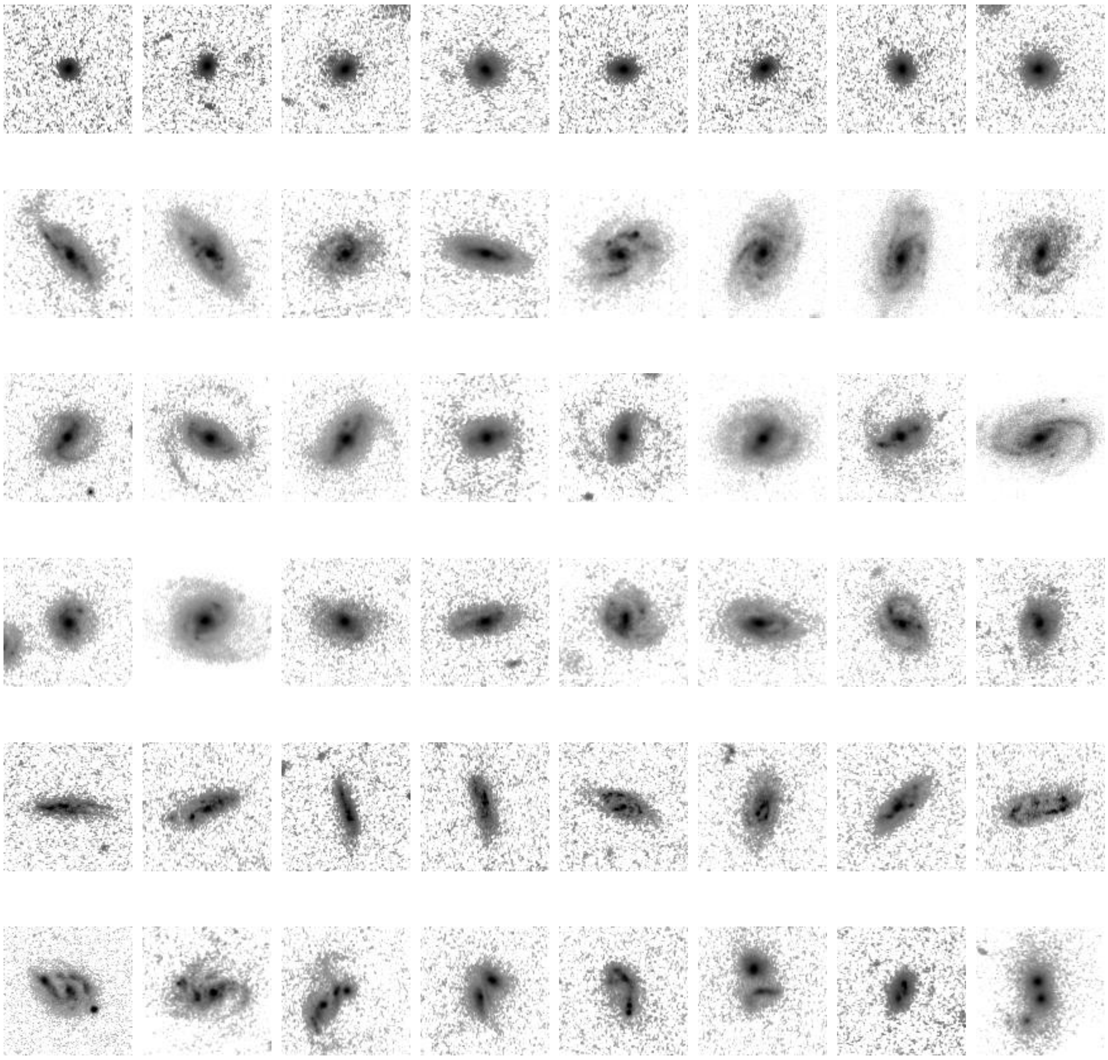

Figure 3.1: Examples of green valley galaxy images in our sample taken with the Hubble Space Telescope (5" × 5" in size). From the top to the bottom rows these galaxies are classified as ellipticals, unbarred disks, strongly barred disks, weakly barred disks, irregulars and merging galaxies.

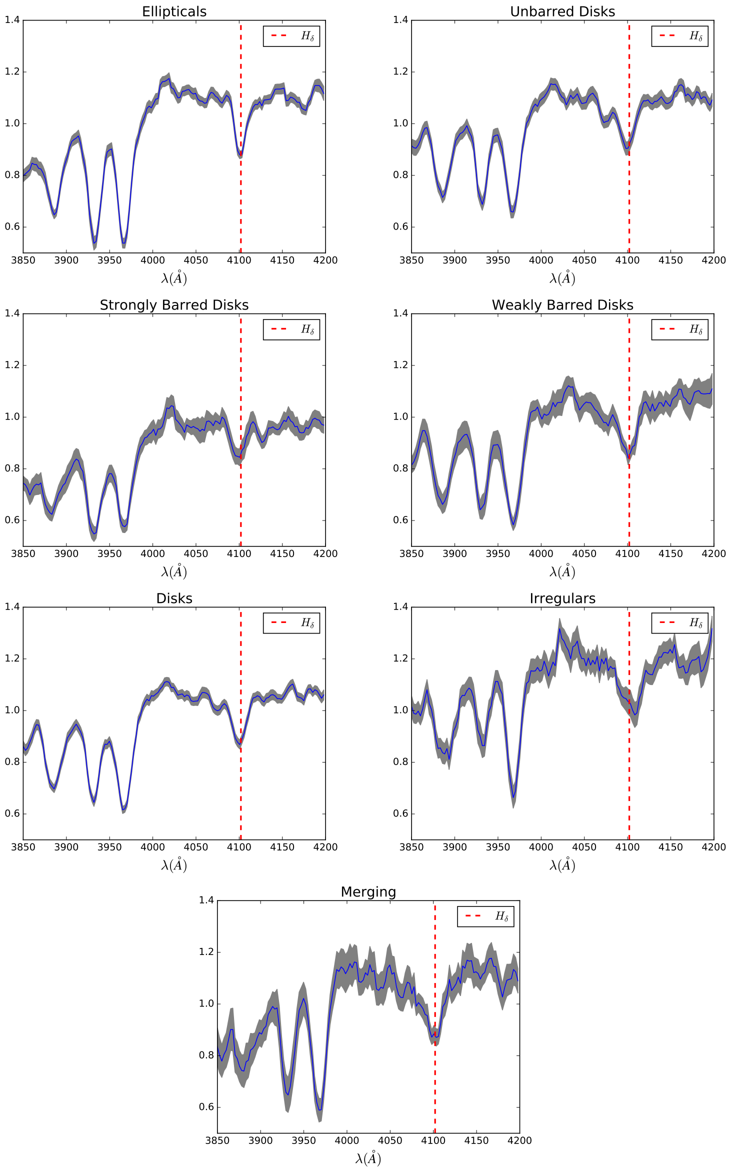

Figure 3.2: Coadded spectra of the zCOSMOS galaxy samples according to morphological type (blue lines). The gray region represents the standard deviation in each pixel. The red line highlights the location of the H_δ absorption line. The y-axes are in units of erg cm^{-2} s^{-1} Å^{-1}.

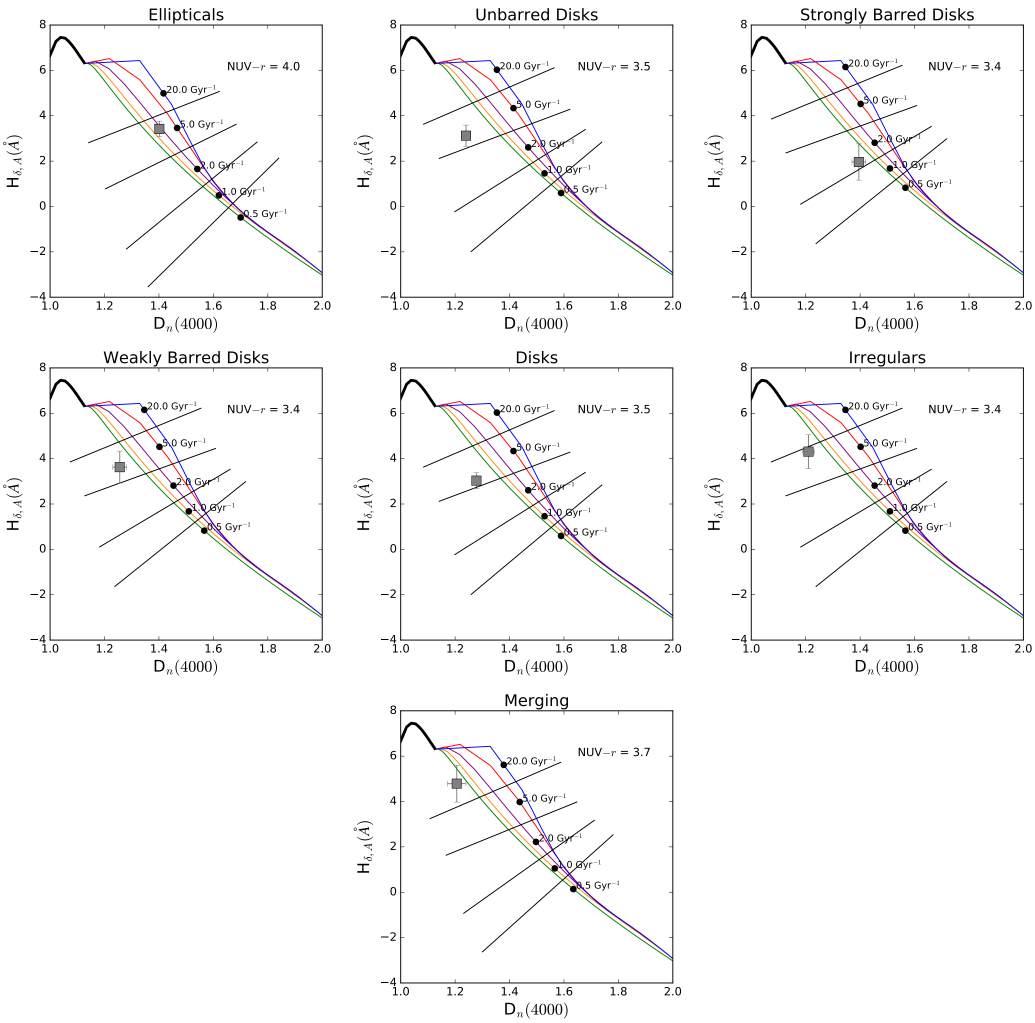

Figure 3.3: Following the same format as that of Figure 2.5, $\mathrm{H}_{\delta,A}\times$ $\mathrm{D}_n(4000)$ diagrams for each morphological type considered in this analysis. Each diagram shows five SFH model curves and the “green valley location” (black points) associated to the median NUV$-r$ color for the sub-sample of galaxies that went into each coadd. The gray squares represents the value of $\mathrm{H}_{\delta,A}$ and $\mathrm{D}_n(4000)$ measured from the coadded spectra for each morphological type. See Section 2.3 for technical details.

Galaxy Type	Number of galaxies	$\langle$NUV$-r\rangle$	γ [Gyr^{-1}]
Unbarred Disks	94	3.5	4.17 ± 0.37
Strongly Barred Disks	15	3.4	1.7 ± 0.24
Weakly Barred Disks	11	3.4	4.79 ± 0.75
Disks	120	3.5	3.66 ± 0.2
Ellipticals	108	4.0	6.08 ± 0.49
Irregulars	48	3.4	8.97 ± 1.73
Merging	20	3.7	20.43 ± 3.64

Table 3.1: Quenching indices and color values for each galaxy type

galaxies undergoing a merger quench their star formation ~5 times faster, with a quenching timescale $\lesssim$50 Myrs. Within the disk classification, the strongly barred galaxies take the longest to have their star formation quenched, with a timescale close to 600 Myrs. Weakly barred and unbarred galaxies transition through the green valley ~3 times faster, with a star formation quenching timescale of ~200 Myrs. Ellipticals and irregulars have on average quenching timescales below 200 Myrs.

3.3 Discussion

We compare our derived star formation quenching timescales with those of Gonçalves et al. (2012), where the authors study a sample of $\gtrsim$ 100 green valley galaxies at $z \sim 0.8$ based on deep individual optical spectra taken with the Keck DEIMOS spectrograph (see Figure 3.5). Although Gonçalves et al. (2012) do not have morphological classifications for their galaxy sample, their results show star formation quenching timescales for a large sample of green valley galaxies within a similar redshift range as probed by our study. Considering that the bulk of our galaxies are classified as disks (~40%) or ellipticals (37%), our results are consistent with those found by Gonçalves et al. (2012), where the γ distribution − with a median value corresponding to ~200 Myrs − displays a clear trend towards the γ values that we determined for these two morphological classes. Consistency of our coadd-

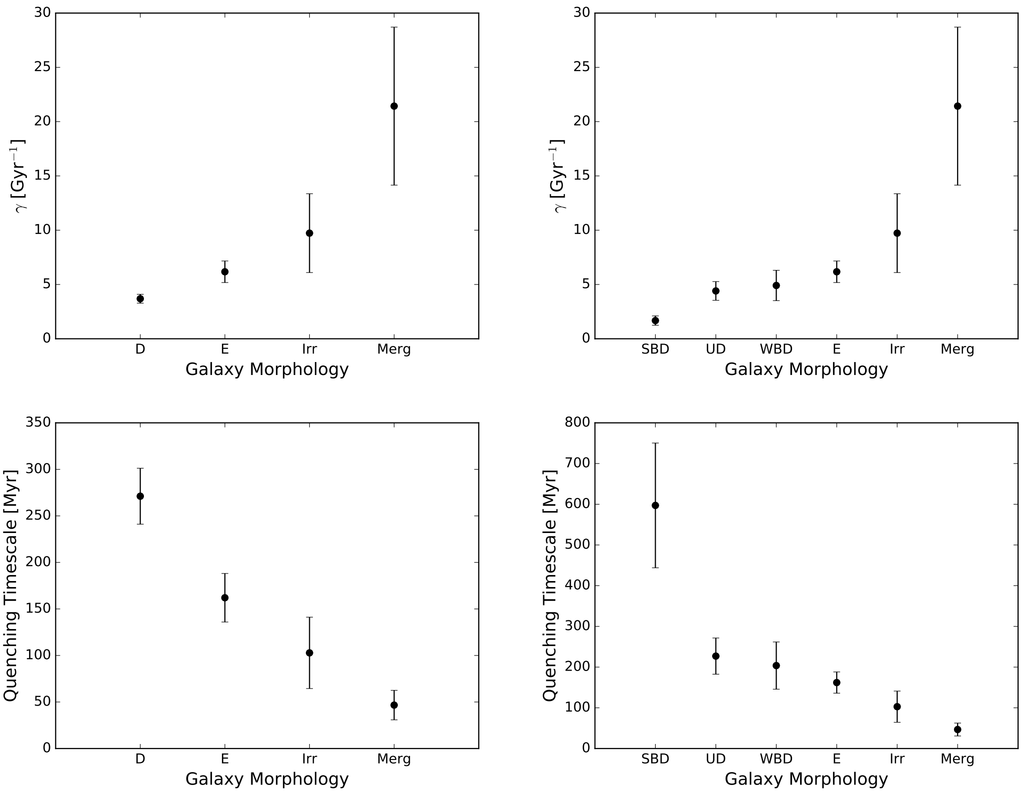

Figure 3.4: ***Top:*** Quenching index (γ) as a function of galaxy morphology. The left panel shows the γ values for the green valley galaxies classified as disk (D), ellipticals (E), irregulars (Irr) and merging galaxies (Merg). In the right panel we divided the disk galaxies into strongly barred disks (SBD), unbarred disks (UD) and weakly barred disks (WBD). ***Bottom:*** Same information as in top panels, but expressed in terms of quenching timescales ($1/\gamma$) in units of Myr. This timescale corresponds to the time when the initial star formation rate has decreased down to $\sim$37% of the initial value.

based work with results based on individual galaxies demonstrates the robustness of our results: although there is likely diversity in star formation quenching timescales within any one morphological class, our coadded spectra reveal representative results as confirmed by comparing with an independent sample selection at similar redshifts.

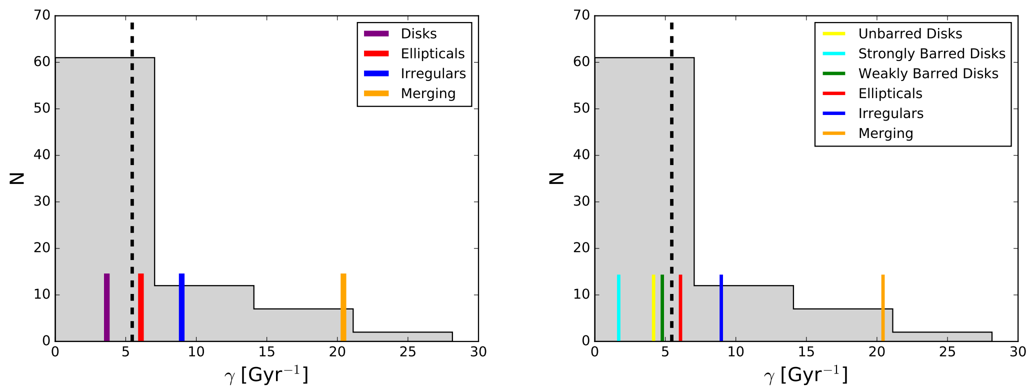

Figure 3.5: Comparison between star formation quenching indices of Gonçalves et al. (2012) and the star formation quenching indices of this work. The histogram represents individual γ values for the sample of Gonçalves et al. (2012); noting that we recalculated them for this work using our exact methodology (see text for details). The vertical dashed line shows the median value for the Gonçalves et al. (2012) sample ($\gamma \sim 5$ Gyr^{-1}) and the short colored lines represent the star formation quenching indices for each morphological type considered in this work. ***Left:*** Comparison with results for disk, elliptical, irregular and merging galaxies from this work. ***Right:*** Comparison with this work, considering the different disk subclasses (strongly barred, weakly barred and unbarred galaxies) independently. Taking the median value of Gonçalves et al. (2012) as separating slow from fast quenching, the disk galaxies seem to be result of slower quenching, whereas elliptical, irregular and merging galaxies quench their star formation faster.

Figure 3.5 shows our results, with star formation quenching timescales of $\gtrsim 250$ Myrs for green valley disks and comparatively shorter values of ~ 150 Myrs, ~ 100 Myrs and ~ 50 Myrs for ellipticals, irregulars and mergers, respectively. This indicates that intense processes – with which the latter morphologies (ellipticals, irregulars and mergers) are typically associated – are 60% to 5 times faster at winding down star formation activity in their host galaxies than disks.

The role of bars as major agents of disk secular evolution has been well established with various lines of observational evidence pointing to an enhancement in central molecular gas concentrations and an ensuing nuclear star formation activity (e.g., Sheth et al., 2005; Ho et al., 1997; Kormendy & Kennicutt, 2004). Among our disk galaxy sub-samples, strongly barred galaxies display the longest star formation quenching timescales. We interpret this not as an indication that the presence of a bar delays in any way the star formation quenching process, but that the mere presence of a strong bar indicates that no other major quenching external agents have affected these galaxies as they transition through the green valley. These strongly-barred green valley galaxies thus represent sites of unencumbered transition from the blue cloud to the red sequence, without any external agent accelerating this process through star formation quenching − neither major merger, nor cluster-related processes, such as harassment and ram-pressure stripping. On the other hand, unbarred and weakly-barred galaxies likely represent disks where external agents may be triggering a more rapid depletion of gas and hence a faster star formation quenching timescale, while interrupting the establishment of a strong bar. Furthermore, unbarred and weakly-barred galaxies may also have specific conditions (gas-richness and dynamical hotness) that on the one hand make them less hospitable towards (strong) bar formation (Athanassoula et al., 2013), but at the same time translate into a more gas-rich turbulent interstellar medium that is conducive to a faster depletion of the available molecular gas.

Systems corresponding to an evolutionary phase that is associated with long timescales are in principle expected to have a significant abundance in the sky. Disks make up almost half of the green valley population ($\sim 40\%$) in our sample, consistent with the longer timescales we determined for their transition from the blue cloud to the red sequence. However, it may come as a surprise that barred galaxies only make up $\sim 9\%$ of the green valley sample, seemingly at odds with their long star formation quenching timescales. However, this scarcity of bars is a reflection of the low bar fraction at these redshifts, where bars make up $\sim 22\%$ of the disk population, with a strong bar fraction of $\sim 9\%$ (Sheth et al., 2008). A drop in the bar fraction has been attributed to a larger proportion of disks being dynamically-hot as we go to higher redshifts, hampering the establishment of bars (Sheth et al., 2012). Within our sample, the fraction of disks with a (strong) bar is (13%) 22%, similar to that of the general disk population at these redshifts. Therefore, although the high fraction of disks that we find in our green valley sample is evidence of their longer quenching timescales, similarly-slow transitioning barred galaxies are simply too few in general at these redshifts to comprise a significant population in our sample.

The coadded spectra of galaxies displaying morphologies consistent with ellipticals, irregulars and mergers point to faster star formation quenching timescales. We note that visual inspection of HST images for our irregular sample (see Figure 3.1) reveals that these galaxies are more akin to clumpy ones at higher redshits. These systems have been found to be quite abundant at $z \sim 1-2$ (Bournaud et al., 2015). The stellar mass of such galaxies is in the range of $10^{10} - 10^{11}$ $M_{\odot}$ and they have been attributed with short gas consumption timescales (Bournaud et al., 2015), consistent with the short star formation quenching timescales we derive (see Figure 3.4). Bournaud et al. (2015) discuss that clumpy galaxies have very irregular morphologies in the optical when compared to nearby spirals of similar mass, because the high gas fractions cause strong gravitational instabilities in the galactic disks, resulting in disk fragmentation and clump formation, with clump masses in the order of $10^8 - 10^9$ $M_{\odot}$. These giant clumps may be at the origin of the formation of bulges in galaxies. However, Puech (2010) argues that clumpy galaxies at $z < 1$ are more stable than those at higher redshifts, suggesting a scenario where interactions between galaxies could be the dominant driver for the formation of clumpy galaxies at $z < 1$. Therefore, they could be coalesced mergers (i.e., mergers in a more advanced stage). Regardless of the clumpy origin, it is expected that these galaxies have very rapid star formation quenching timescales.

The fraction of elliptical galaxies in our green valley sample ($\sim$37%) is almost as high as the fraction of disk galaxies (40%), suggesting that the physical processes responsible for elliptical galaxy formation are common. It has been widely established that the characteristically old stellar population associated to the bulk of the stellar content in massive ellipticals formed in a single event in the distant past, likely a major merger (Toomre, 1977). Merger simulations indicate that the interaction between colliding gas-rich spirals may extend over $\sim 1-2$ Gyr (e.g., Springel et al., 2005; Conselice, 2006)), with a sudden burst of star formation lasting $\sim 10^8$ yr. Together with the suggestion by Peng et al. (2010) that galaxy mergers are one of the main mechanisms to quench star formation at $z > 0.5$, the abundance of this morphological class may be explained with a galaxy merger origin. Applying an exponential decay model for star formation rates on SDSS photometric data, Schawinski et al. (2014) reached a similar conclusion where elliptical galaxies at low redshifts quench their star formation activity through mergers.

We find increasingly short timescales for the elliptical, irregular and merger morphological classifications and interpret them as reflecting three different time-averaged perspectives of a sequence of a major galaxy fusion. We attribute this to the fact that we are measuring the *average* star formation quenching timescales for each galaxy type from the galaxy spectra and photometry. The set of galaxies composing our "merger" sample corresponds to systems caught early-on in a merger sequence, when interacting members are still distinguishable from each other. Rest-frame NUV$-r$ colors place these systems within the green valley and the short quenching timescales are a reflection of a short-lived peak and drop in star-formation that triggers a rapid change in the system's color. Irregulars may in turn correspond to a more advanced merger phase, when the interacting galaxies have coalesced to a single, disturbed system that displays multiple knots likely corresponding to the merging galactic nuclei. The average star formation quenching timescale hence does not merely include a sharp change in color, but a phase in which the coalesced system likely does not alter significantly its global color. Lastly, the galaxies with spheroidal morphology $-$ classified as ellipticals $-$ denote the end-point stage of a post-merger system with no remaining morphological signature of a past interaction. Considering that the rest-frame, dust-corrected colors of these galaxies place them within the green valley region of the CMD, we are catching them at a transitional stage. While galaxies caught at an early merger stage are in the midsts of a very sharp change in global color, irregulars and $-$ more significantly $-$ ellipticals trace a more diluted change in color due to a merger in their recent past. The proportion of these galaxy types $-$ mergers (7%), irregulars (17%) and ellipticals (37%) $-$ within our green valley sample are consistent with a picture where these three morphological classifications trace three distinct stages in a merger sequence, with increasingly longer lifetimes. With an increase rate in merger activity (Lotz et al., 2011), the abundance of clumpy galaxies and merger-like morphologies in the green valley is expected to increase with redshift.

Based on the analysis of SDSS photometry for green valley galaxies at $z \sim 0.2$, Schawinski et al. (2014) suggested secular evolution and mergers as the two main scenarios for star formation quenching at low redshift. With $\sim 80\%$ of our green valley sample represented by ellipticals and disks in similar proportions ($\sim 37\%$ and $\sim 40\%$, respectively), our results at intermediate redshifts ($z \sim 0.5-1$) are consistent with both of these agents being important drivers of the galaxy color transition at higher redshifts, at least at $z < 1$. However, our quantification of the star formation quenching timescale as a function of morphology indicates that although secular evolution may ultimately lead to gas exhaustion in the host galaxy via bar-induced gas inflows that trigger star formation activity, secular agents are not major agents in the rapid quenching of galaxies at these redshifts. Galaxy interaction, associated with the elliptical, irregular and merger morphologies contribute, to a more significant degree, to the fast transition through the green valley at these redshifts.

Chapter 4

Star Formation Quenching as a Function of Compactness

Red sequence galaxies are typically more centrally-concentrated at a given mass when compared to blue cloud galaxies (e.g., Cheung et al., 2012; Fang et al., 2013). This suggests that independently of which galaxy-wide agents (e.g., bar/spiral structure, AGN, merger) transforms star-forming galaxies as they transition through the green valley, they must cause compaction in host galaxies. Star formation quenching is thus argued to be accompanied necessarily by an increase in the compactness of galaxies.

Among red passive galaxies there is a group of galaxies that are characterized for being very compact and massive, called *red nuggets*. The number density of red nuggets reaches a peak around $z \sim 1.5$ and decreases at lower redshifts (e.g., van der Wel et al., 2014; van Dokkum et al., 2015; Charbonnier et al., 2017). Moreover, a population of compact star-forming galaxies (*blue nuggets*) is largely found at $z = 2 - 3$ and then practically disappears at $z = 1 - 1.5$ (e.g., Barro et al., 2013). This suggests that blue nuggets experience very fast star formation quenching and also these objects are not produced at lower redshifts.

Although the redshift distribution of blue and red nuggets suggests that these galaxies transition through the green valley at $z > 1$, a significant number of green valley compact galaxies (*green nuggets*) are found at $0.5 < z < 1.0$. We study this population, focusing on measuring the star formation quenching timescales of these green nuggets. We compare them to less compact counterparts, with the objective of understanding how compactness is correlated with faster quenching timescales. In this Chapter we describe our sample selection for this specific study, defining ultra-compact, compact and normal-sized galaxies. We study star formation quenching timescales in the light of the typical galactic processes associated with red nuggets that are much more common at earlier times.

4.1 Compactness Definition

A variety of definition for compactness exists in the literature (e.g., Carollo et al., 2013; Quilis & Trujillo, 2013; van Dokkum et al., 2015), based on different measures. For this work, we apply the compactness definition proposed by van der Wel et al. (2014):

$$R_{\rm eff} < A \times \left(M_\star/10^{11}\,M_\odot\right)^{0.75} \ , \tag{4.1}$$

where $R_{\rm eff}$, in units of kpc, is the effective radius (containing half of the total flux), $M_\star$ is the galaxy stellar mass, and $A = 1.5$ or 2.5 kpc define ultra-compact and compact galaxies, respectively.

We estimate the effective radius $R_{\rm eff}$ using the following conversion:

$$R_{\rm eff} = D_A(z) \times R_{GIM2D} \tag{4.2}$$

where $D_A(z)$ is the cosmological angular distance and R_{GIM2D} is the PSF-convolved half-light radius of the object. This information is taken from the ZEST catalog (Chapter 3, Sargent et al., 2007).

4.2 UltraVISTA Catalog

To define our sample of compact, massive green valley galaxies, we obtain stellar masses from the UltraVISTA catalog (McCracken et al., 2012). This catalog provides photometry in 30 bands, from UV to near-IR, including data from GALEX (Martin et al., 2005), CFHT/Subaru (Capak et al., 2007), UltraVISTA (McCracken et al., 2012) and S-COSMOS (Sanders et al., 2007). The authors determined the stellar population parameters (including stellar mass) by fitting the galaxy spectral energy distribution (SED) through the FAST code (Fitting and Assessment of Synthetic Templates, Kriek et al., 2009). This code uses the Bruzual & Charlot (2003) models, assuming solar metallicity, Chabrier (2003) initial mass function and the Calzetti et al. (2000) dust extinction law.

4.3 Environment Catalog

We obtain the local density of the green valley galaxies from Darvish et al. (2015). They derived the local environment using the weighted version of the Voronoi tessellation method (weighted adaptive kernel, Darvish et al., 2014) in a $K_s < 24$ sample in the COSMOS field (Capak et al., 2007), with photometric redshifts from the UltraVISTA catalog (McCracken et al., 2012; Ilbert et al., 2013) at $0.1 < z < 3.0$.

In order to estimate the local environment Darvish et al. (2015) built a series of redshift slices on the sample. The widths of the slices are obtained from the probability distribution function (PDF) of the galaxies: for each slice, the width is defined as twice the median redshift uncertainty of the galaxies at each redshift.

Basically, the weighted adaptive kernel method consists of assigning a region (area) to each galaxy. The area A_i at the position of the ith galaxy is inversely proportional to the local density (higher density means smaller area). Therefore, the local density $\Sigma(r_i)$ is given by:

$$\Sigma(r_i) = \frac{1}{A_i} \ . \tag{4.3}$$

The galaxy environment is a function of the redshift, because the structures of the universe grow and change with cosmic times. In this case, one useful quantity is the *overdensity* $(1 + \delta_i)$, defined as the local surface density $\Sigma(r_i)$ divided by the median local surface density Σ_{median} within each z-slice, at the position of the ith galaxy:

$$1 + \delta_i = \frac{\Sigma(r_i)}{\Sigma_{\text{median}}} \ . \tag{4.4}$$

We use the overdensity quantity $(1 + \delta)$ do describe the local density of the green valley galaxies.

Compactness	Number of galaxies	$\langle$NUV$-r\rangle$	γ [Gyr^{-1}]
Normal-sized	311	4.06	3.05±0.03
Compact	25	4.35	7.41±1.28
Ultra-compact	3	4.24	14.0±4.86

Table 4.1: Number of galaxies, median color values and quenching index for each compactness type.

4.4 Results

We select normal-sized, compact and ultra-compact green valley galaxies at the redshift range of $0.5 < z < 1.0$ according to Equation 4.1, where normal-sized galaxies are defined as $A > 2.5$. We have chosen galaxies with the stellar mass $M_\star > 10^{10.7}$ $M_\odot$, that is the condition by the estimator adopted in this work (van der Wel et al., 2014).

The Figure 4.1 shows the overdensity $(1 + \delta)$ distribution for normal-sized, compact and ultra-compact green valley galaxies. In an effort to isolate the influence of environment, we exclude from our analysis green valley galaxies in environments characterized as high overdensities. According to Darvish et al. (2015) high overdensity is defined as $(1+\delta) > 3.0$ and low overdensity is $(1+\delta) < 1.5$. To maintain a reasonable number of galaxies with zCOSMOS spectra, for this present analysis we select green valley galaxies in low-to-moderate environment $(1 + \delta < 2.0)$. In total we select 311 normal-sized, 34 compact and 5 ultracompact green valley galaxies.

We have checked the HST galaxy images of the compact and ultra-compact and we verify that some galaxies have a nearby companion. To make our results robust we exclude the galaxies whose line of sight had another galaxy. The resulting final numbers of normal-sized, compact and ultra-compact galaxies are shown in Table 4.1.

Based on the need for high S/N to determine star formation quenching timescales, we follow the same approach described in Chapter 2 and produce a coadded spectrum for each compactness sub-sample: normal-size, compact and ultra-compact. The resulting green valley coadded spectra for each compactness

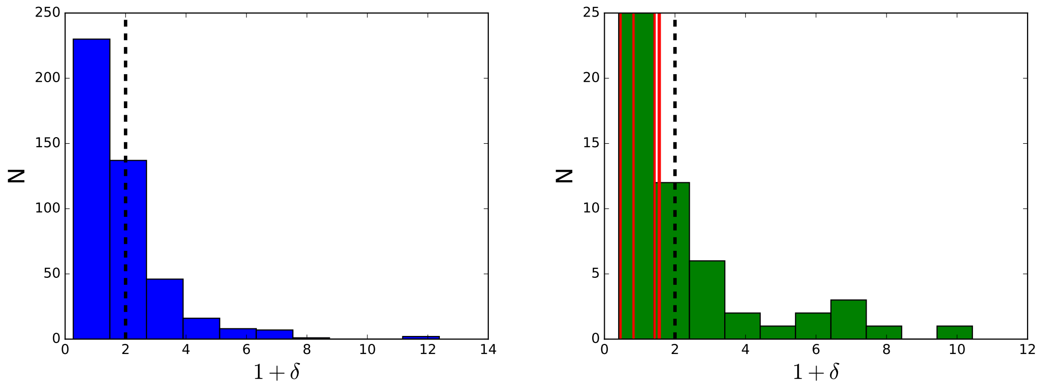

Figure 4.1: Overdensity distribution for normal-sized (left) and compact and ultra-compact (right) green valley galaxies which have zCOSMOS spectra. On the right Panel the compacts are represented in green and ultra-compacts are represented by red vertical lines. The vertical dashed black line in each Panel delimits the overdensity limit for low-to-moderate environments ($1 + \delta < 2.0$).

classification are shown in Figure 4.3. Following the mass and size cuts and excluding possible interactions with other galaxies, together with the availability of zCOSMOS spectra, only 3 green valley galaxies comprise the sample of ultra-compact. In principle, we would not be able to calculate the $H_{\delta,A}$ and $D_n(4000)$ spectral indices. However, these galaxies are fortunately bright sources, with a average m_r value of 22.5. Using the Exposure Time Calculator from ESO we reproduced the galaxy spectrum for such bright sources with the conditions of zCOSMOS, described in Chapter 2. The reproduced spectrum is shown in Figure 4.2. With a S/N$\sim$ 5, the coaaded spectrum of the 3 ultra-compact green valley galaxies (Figure 4.3) is sufficient to allow us to determine the H_δ and $D_n(4000)$ spectral indices (see Appendix A)

In Figure 4.4 we show the results of our measurements within the $H_{\delta,A} - D_n(4000)$ diagram for the 3 coadded spectra shown in Figure 4.3. From these results we determine the star formation quenching indices (γ) for each compactness sample. These, their corresponding uncertainties, as well as average NUV$-r$ colors are also shown in Table 4.1. Figure 4.5 shows a direct comparison of star formation quenching indices and timescales for all 3 bins of compactness.

The star formation quenching timescales of green nuggets from our sample

(Figure 4.5) are in agreement with timescales from previous studies with compact galaxies (Barro et al., 2013; Zolotov et al., 2015). Particularly, these authors claim that the transition from blue to red nugget must lasts $\sim$ 500 Myr.

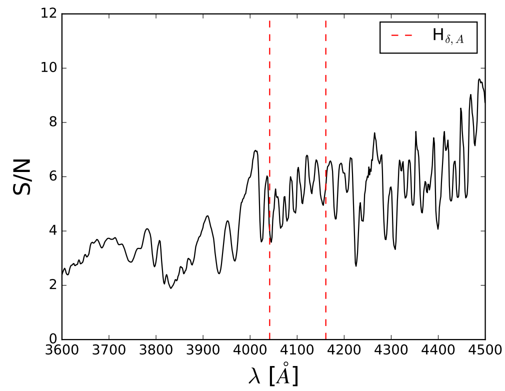

Figure 4.2: Signal-to-noise as a function of wavelength for a $m_r \sim 22.5$ point source. The red vertical dashed lines delimit the H_δ absorption on the galaxy spectrum.

4.5 Discussion

We find that compact and ultra-compact galaxies quench their star formation $\sim 2-5$ times faster than their normal-sized counterparts (see Figure 4.5). Based on the redshift distribution of the red and blue nuggets, Barro et al. (2013) estimate that the transition from blue to red lasts $\sim$ 500 Myrs. Considering that our γ values reflect when the initial star formation rate decreases to 37% of the initial value, our findings point to a green valley transition for compact and ultra-compact galaxies that may last $\sim 200-450$ Myrs, consistent within the uncertainties of Barro et al. (2013). Furthermore, at the peak of compactness, cosmological simulations of the quenching and compaction of high-z galaxies by Zolotov et al. (2015) show that the gas depletion timescale is very short, $\sim$ 100 Myr, consistent with the quenching timescales associated with the most extreme ultra-compact subsample in our analysis.

Similarly to our previous analysis (Chapter 3) we compare our results to the distribution of quenching timescales for individual galaxies at intermediate redshifts determined by Gonçalves et al. (2012), where these authors studied a sample of

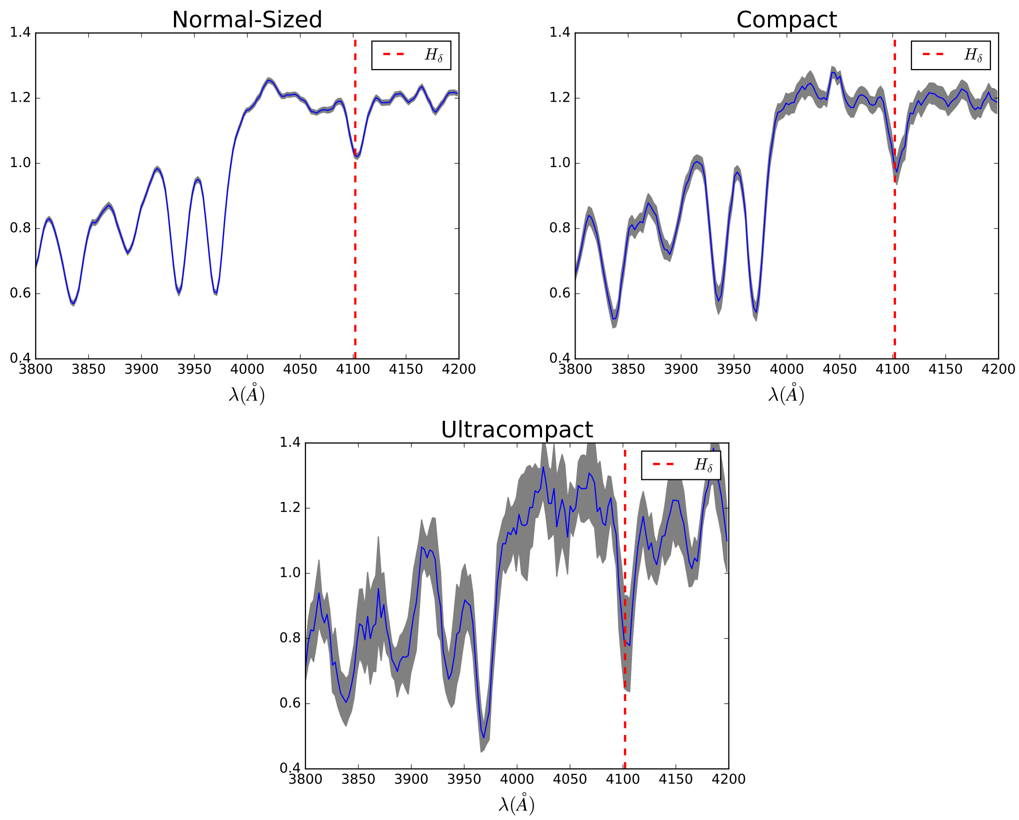

Figure 4.3: Coadded spectra of the zCOSMOS galaxy samples according to compactness (blue lines). The gray region represents the standard deviation in each pixel. The y-axes are in units of erg cm^{-2} s^{-1} Å^{-1}.

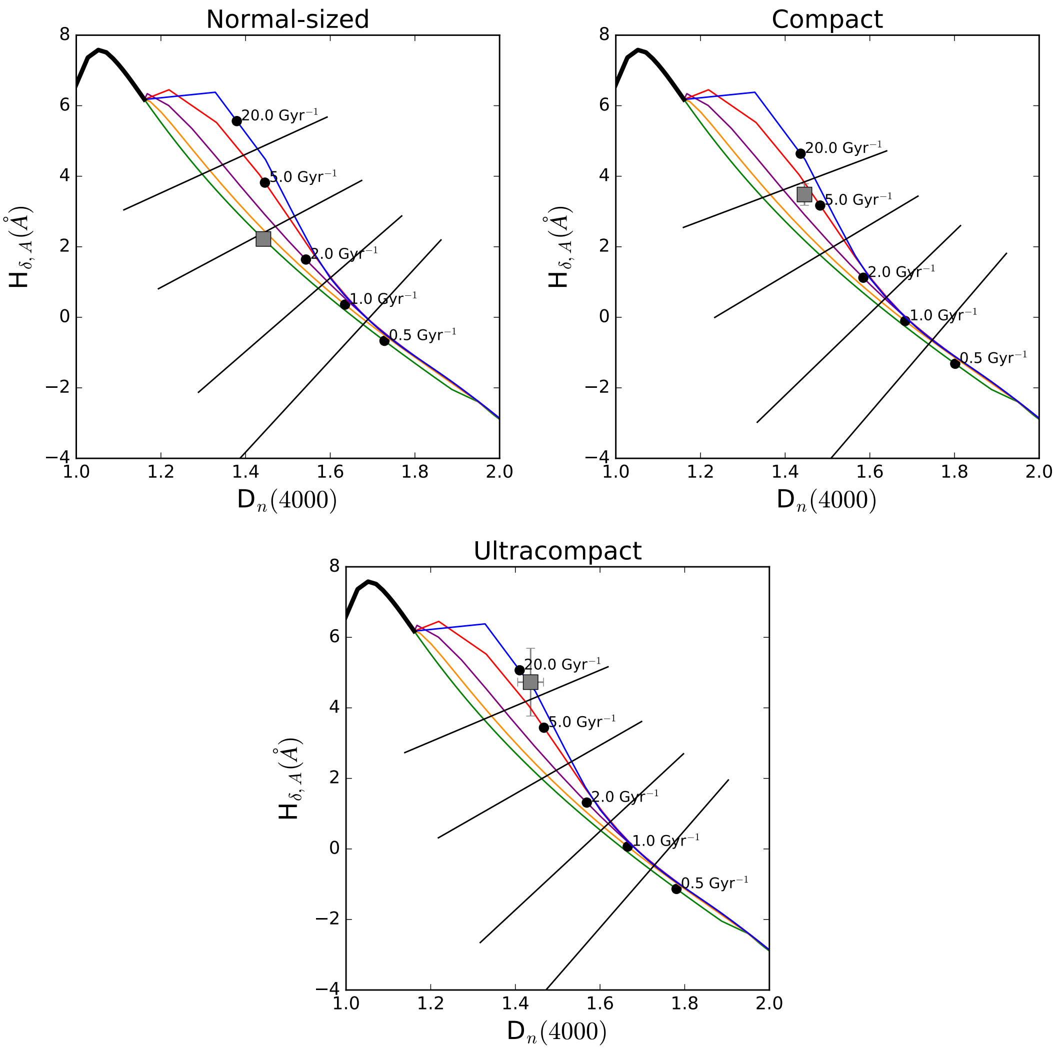

Figure 4.4: $H_{\delta,A}\times$ $D_n(4000)$ plane and indices (gray squares) for each galaxy compactness. The black dots represent the $D_n(4000)$ and $H_{\delta,A}$ values in each SFH model when it reaches the average NUV$-r$ color specified in the Table 4.1. The error bars is the standard deviation of the indices. The straight lines represent the geometric mean in two consecutive SFH models.

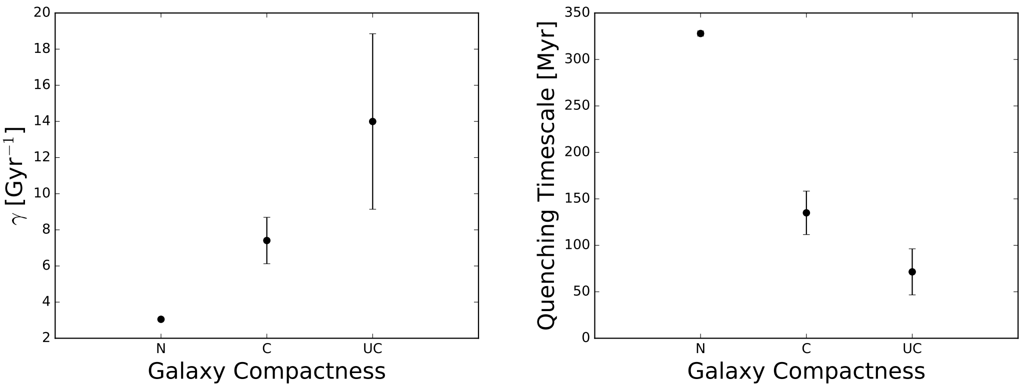

Figure 4.5: ***Left:*** The exponential index (γ) values for the green valley galaxies classified as normal-sized (N), compact (C) and ultra-compact (UC). ***Right:*** Quenching timescales when the initial star formation rate decreases to $\sim$37% of the initial value ($1/\gamma$).

$\gtrsim$ 100 green valley galaxies at $z \sim 0.8$ based on deep individual optical spectra taken with the Keck DEIMOS spectrograph (Figure 4.6). Considering that the bulk of the galaxies in our sample are normal-sized, the observed agreement between the coadd-based result for this subsample and the typical values found by Gonçalves et al. (2012) represent a good sanity check. On the other hand, compact and ultra-compact galaxies display star formation quenching timescales that place them on the tail of the Gonçalves et al. (2012) distribution, consistent with faster quenching.

We analyze the distribution of compactness as a function of NUV$-r$ color and redshift in order to study the evolution of the fraction of green nuggets with cosmic time and as a function of position within the green valley. Figure 4.7 show our analysis.

We find that the fraction of green nuggets increases with galaxy color, indicating that the majority of compact objects occupy the redder part of the galaxy CMD. We also identify a clear trend with redshift, where the green nugget population becomes more significant at early times, going from $\sim 5\%$ at $z \sim 0.6$ to $\sim 20\%$ at $z \sim 0.9$. This is coherent with the observed increase in the blue nugget fraction at higher redshifts by Barro et al. (2013), which suggests that the transformation of blue nuggets to red ones $-$ and hence the prevalence of green nuggets $-$ was more common at higher redshifts; as blue nuggets traverse the green valley (in the form

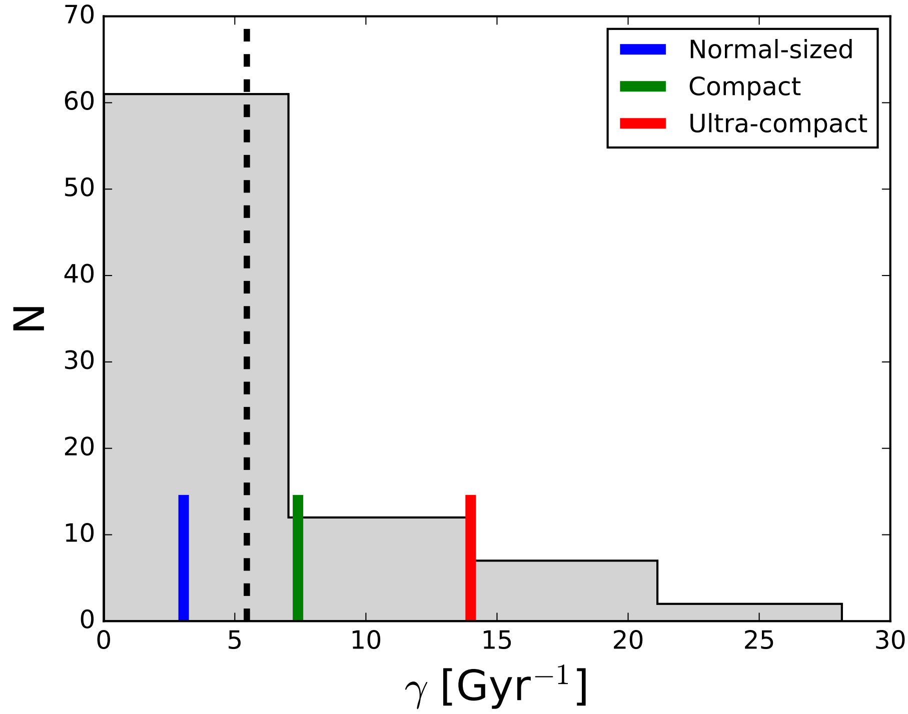

Figure 4.6: Comparison between star formation quenching indices of Gonçalves et al. (2012) and the star formation quenching indices for this present analysis. The vertical dashed line represents the median value for the Gonçalves et al. (2012) sample ($\gamma \sim 5$ Gyr^{-1}) and the colored full lines represent the average star formation quenching indices for normal-sized, compact and ultra-compact green valley galaxies. Taking the median value of Gonçalves et al. (2012) as separating slow from fast quenching, the normal-sized galaxies seem to be result of slower quenching, whereas compact and ultra-compact galaxies quench their star formation faster.

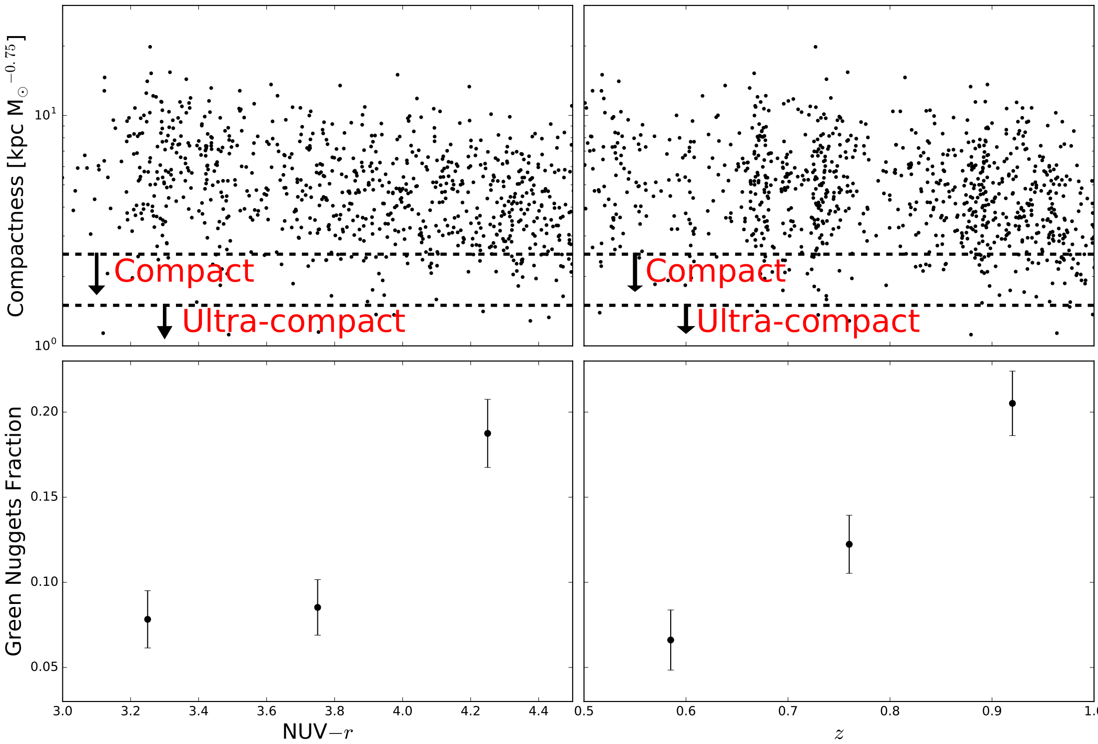

Figure 4.7: ***Top:*** Compactness as a function of NUV$-r$ (left panel) and redshift (right panel) of green valley galaxies in our sample. The black arrow in each panel indicates the direction for higher compaction (i.e., the smaller the compactness value, the more compact the galaxy is). The top dashed line delimits compact galaxies from normal-sized ones and the bottom dashed line delimits ultra-compact galaxies from the compact ones. ***Bottom:*** Green nugget fraction as a function of NUV$-r$ and redshift.

of green nuggets) and settle within the red sequence (as red nuggets), the fraction of green nuggets is expected to ultimately drop, reflecting a decrease in number density with cosmic times.

The principal mechanisms involved in the formation and evolution of compact galaxies have been widely discussed in the literature. Dekel & Burkert (2014) elaborated a toy-model suggesting that the formation and evolution of compact galaxies at high redshifts involve the following phases:

- **Violent disk instability phase:** The high gas fraction ($> 50\%$) typically found in high-z galaxies causes strong gravitational instabilities in galactic disks. Briefly, the instability arises when the centrifugal and thermal forces in the disk are not in equilibrium with the gravitational force. The violent disk instability (VDI) results in disk fragmentation, causing the formation of giant clumps, with individual clump masses of $\sim 10^{8-9}$ $M_\odot$ (Bournaud et al., 2007; Ceverino et al., 2010, 2012).

- **Blue nugget phase:** In this phase the giant clumps rapidly migrate towards the center of the host galaxy, producing a compact gas-rich object (i.e., blue nugget) in $\sim 300 - 500$ Myrs (Bournaud et al., 2007). The peak of star formation rate can reach ~ 100 $M_\odot$ yr^{-1} (Zolotov et al., 2015).

- **Green nugget phase:** Star formation activity is quenched during this phase. Many quenching mechanisms may be present simultaneously, including stellar feedback (Murray et al., 2005; Lagos et al., 2013), quasar-mode feedback from an active galactic nucleus (AGN) (Ciotti & Ostriker, 2007; Di Matteo et al., 2005; Schawinski et al., 2009) and morphological quenching (Martig et al., 2009). These mechanisms are associated to a *fast mode*. Additional mechanisms can act in *maintenance mode* (avoiding new star formation activity), such as virial shock heating and radio mode AGN feedback (Dekel & Birnboim, 2006; Croton et al., 2006; Cattaneo et al., 2009).

- **Red nugget phase:** Red passive compact galaxies are formed during this phase. These objects can grow their sizes due to minor mergers and/or adiabatic expansion (Barro et al., 2015) at later times.

This toy model is consistent with the observed redshift distributions of blue and red nuggets informed by Barro et al. (2013), Barro et al. (2015) and Charbonnier et al. (2017). Furthermore, recent cosmological simulations of high-redshift galaxies by Zolotov et al. (2015) back up these toy-model predictions.

The formation of blue nuggets, and consequently the evolution in their internal properties are more likely to occur at high redshift, where the amount of available cold gas is much higher than in local galaxies (Tacconi et al., 2010; Genzel et al., 2010). Figure 4.8 displays an evolutionary scenario proposed by Barro et al. (2013), where galaxies evolve via one of two principal tracks: the *early-track*, that happens at early times ($z = 2 - 3$) and; the *late-track*, that is more common at late times ($z = 0 - 2$).

In the early-track the principal mechanisms involved are the ones described by the Dekel & Burkert (2014) toy-model. Particularly, the star formation quenching in green nuggets is most likely due to a combination of fast mode and maintenance mode processes. Additionally, Barro et al. (2013) discuss the role of the early-track as a means to explain on the one hand the growth of AGNs in blue nuggets − leading to the observed coexistence of AGN and star-formation activity in these galaxies (Aird et al., 2010) − and on the other hand, the establishment of the Magorrian relation, where the stellar velocity of the galaxy spheroid is correlated with the mass of the underlying supermassive black hole (Magorrian et al., 1998; Ferrarese & Merritt, 2000; Gebhardt et al., 2000; Tremaine et al., 2002)

In the late-track, the processes involved in the Dekel & Burkert (2014) toy-model do not occur commonly in galaxies because the gas-fraction is much lower at later times. Within this track star formation is quenched at a slower pace in green valley galaxies with larger spatial extensions. Considering both tracks, the resulting red sequence is formed by a mixture of compact galaxies (formed along the early track) and of extended ones (formed along the late track). Recently, recent works demonstrated that the number density of compact red sequence galaxies reach a peak around $z \sim 1.5$ van der Wel et al. (e.g., 2014); **?**, decreasing towards lower redshifts. This suggests that compact red galaxies are continuously growing their size, probably through minor mergers (Naab et al., 2009), formation of a star-forming disk surrounding the compact passive galaxy (Zolotov et al., 2015) and adiabatic

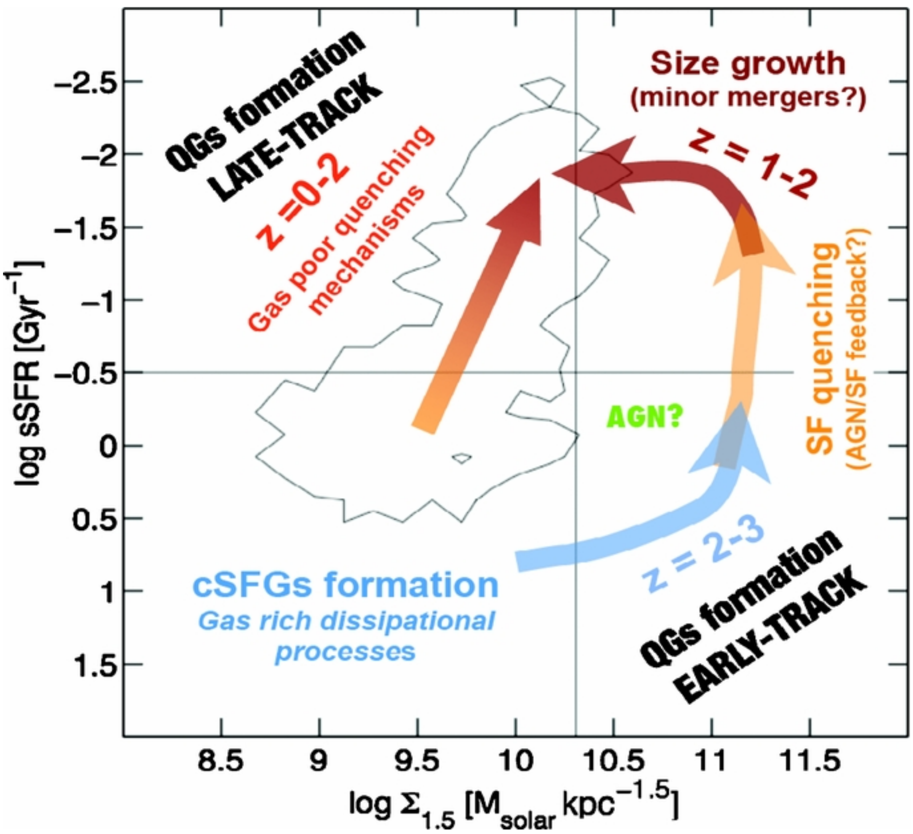

Figure 4.8: Specific star formation rate (SFR/M$_\star$) as a function of compactness (M$_\star/r^{1.5}$), showing two possible evolution paths for red sequence formation (Barro et al., 2013): the early-track and the late-track. At early times ($z = 2 - 3$, early-track) the formation of compact galaxies is common due to gravitational instabilities caused by high gas fractions. Fast mode and maintenance processes quench star formation in green nuggets very quickly. Once in the red sequence, the red nuggets grow their sizes over time. At $z < 2$ mechanisms that impact normal-sized galaxies become more important, including secular evolution, gas-poor mergers and environment processes. The black contour shows the galaxy distribution in the local universe.

expansion caused by stellar mass loss (Damjanov et al., 2011; Furlong et al., 2017; Wellons et al., 2016).

At the redshifts of our study, $0.5 < z < 1.0$, the majority of compact galaxies are passive − that is, most nuggets are already red nuggets formed via early-track at early epochs. We identify an increase in the fraction of green nuggets towards early times in this range, which indicates that transitional green compact galaxies become more common. Consistent with the early-track red sequence formation scenario, at early times we expect that galaxies may be more gas-rich and, consequently, more prone to disk instabilities, compaction and rapid quenching, following the scenario proposed by Dekel & Burkert (2014). However. the rapid quenching timescales that we measure for our compact and ultra-compact green valley galaxies suggest that although early-track red sequence formation was likely more significant at higher redshifts, it can still act at $z < 1$.

Chapter 5

Star Formation Quenching as a Function of AGN Activity

The typical mass of galaxies transiting from the blue cloud to the red sequence decreases over cosmic times (Bundy et al., 2006; Gonçalves et al., 2012; Juneau et al., 2005) and less massive galaxies have more extended star formation histories. This is a strong indication of the *downsizing* picture, where the most massive galaxies reach the red sequence earlier than lower massive ones (e.g., Cowie et al., 1996).

What mechanism could be driving massive galaxies rapidly towards the red sequence? Many authors have pointed to the need for feedback from an active galactic nucleus to supply the energy required to stop star formation activity in host galaxies (Cattaneo et al., 2009; Ciotti & Ostriker, 2007; Dubois et al., 2013; Springel et al., 2005). This scenario is also supported by the well-established correlation between the velocity dispersion of a massive galaxy's spheroid and the mass of an underlying central supermassive black hole (SMBH, Magorrian et al., 1998; Tremaine et al., 2002; Häring & Rix, 2004; Gültekin et al., 2009; Graham & Scott, 2013).

The amount of energy released by the AGN feedback during the SMBH accretion can be partially absorbed by the host galaxy, heating and/or ejecting the gas and, consequently, leading to a decrease in star formation activity (e.g., Springel et al., 2005).

In this Chapter we identify a population of AGN green valley galaxies at $0.5 < z < 1.0$ and measure their star formation quenching timescales following the same approach described in Chapter 2. We use galaxies with no AGN signatures as a control sample and compare the star formation quenching timescales of both samples to assess the impact that AGN may have in galaxies during their transition through the green valley at intermediate redshifts.

5.1 Active Galactic Nuclei Catalogs

Optical selection of AGNs has traditionally received great attention based on the broad availability of rest-frame optical spectra for low-redshift systems (e.g, SDSS) and the development of efficient AGN diagnostics (e.g., BPT diagram; Baldwin et al., 1981). However, at higher redshifts, sample sizes with deep rest-frame optical spectra are severely reduced. Hence, we here focus on AGN selection based on other wavebands.

AGN signatures are identified in different wavebands depending on the intrinsic properties of the system. Typically, to have a more complete census of the AGN population it is necessary to combine different selection methods. For instance, although the majority of AGN sources can be identified in the X-rays, the soft X-ray photons (< 10 keV) can be absorbed by the intervening obscuring torus (Griffith & Stern, 2010). Radio and mid-IR emissions are less susceptible to dust extinction, and thus very useful to identify both unobscured and obscured AGNs. Combining AGN selection at these different wavelengths, we are better positioned to address the question of the AGN's impact in quenching star formation in the host galaxy.

In this present work we select AGN green valley galaxies from two catalogs: (1) a compilation of AGN catalogs with observations in radio, mid-infrared and X-ray wavelengths (Griffith & Stern, 2010); and (2) the Chandra COSMOS-Legacy survey (Civano et al., 2016; Marchesi et al., 2016).

1. Griffith & Stern (2010) provide a unified catalog of the COSMOS field that contains AGN candidates identified in the radio (372 in VLA-COSMOS large project, Schinnerer et al., 2007), X-ray (1360 in XMM-Newton COSMOS survey, Hasinger et al., 2007; Cappelluti et al., 2009) and mid-infrared (1238 in S-COSMOS survey, Sanders et al., 2007).

2. The Chandra COSMOS-Legacy survey is a 4.6 Ms Chandra program that has

imaged the entire COSMOS field with an effective exposure of ~160 ks over the central COSMOS area (1.5 deg^2) and of ~80 ks in the remaining area. The final catalog comprises 4016 sources, detected in at least one of the following three bands: full (0.5–7 keV), soft (0.5–2 keV) and hard (2–7 keV). A source detected in both the soft and hard is considered to be an AGN. We cross correlate our catalog of green valley galaxies (defined in Chapter 2) with the Chandra COSMOS-Legacy catalog from Marchesi et al. (2016).

5.2 The VLT LEGA-C spectroscopic survey

In this present study we also exploit the first data release of the VLT LEGA-C spectroscopic survey (LEGA-C, van der Wel et al., 2016). LEGA-C is a four-year project which will produce deep spectra (20 hrs long integrations) for $\sim$ 3200 galaxies with $M_\star > 10^{10}$ $M_\odot$ at $0.6 < z < 1.0$. The observations are taken with VIMOS instrument, located at ESO VLT. The spectral coverage of LEGA-C spectra is from 6300Å to 8800Å, with a resolution of $R \sim 2500$.

The individual galaxy spectra in LEGA-C survey have sufficient S/N to implement our methodology described in Chapter 2 and, hence, determine the star formation quenching timescales in individual green valley galaxies. Taking advantage of the first set of LEGA-C data released on September, 2016, we extended our star formation quenching methodology to available green valley LEGA-C targets. This enable us to compare our zCOSMOS coadd-based results with a set of individual galaxy measurements. This is a first step to go beyond determining typical quenching timescales for select green valley galaxy populations (with and without AGNs in this case) and to start probing the diversity present within each population.

5.3 Results

From a total of 638 green valley galaxies at $0.5 < z < 1.0$ with zCOSMOS spectra, 42 present AGN signatures following the two AGN catalogs described in Section 5.1. As in Chapter 4 we include as part of our discussion the potential effect of the environment. For this reason we consider our results concerning the role of AGNs both for the entire sample regardless of the local galaxy number density and for a sample limited to 443 green valley galaxies located in low-to-moderate environmental overdensities ($1 + \delta < 2$). Figure 5.1 shows the stellar mass distribution of our AGN and non-AGN green valley samples, for the sample regardless of the environment and for a subsample that excludes high-density environments.

As part of our analysis we produce a coadded spectrum (following the methodology described in Chapter 2) for each of three stellar mass bins within the AGN and non-AGN samples. We have chosen the stellar mass bins in order to maintain approximately the same number of AGN galaxies in each bin (see Figure 5.1); we adopt the same stellar mass bin definition for the non-AGN sample in order to make an adequate comparison to the AGN counterparts. Tables 5.1 and 5.2 show the sample distribution of non-AGNs and AGNs in stellar mass bins considering all environments; Tables 5.3 and 5.4 show this for galaxies in environments with low-to-moderate overdensities. The coadded spectra are shown in Figures 5.2 and 5.3, considering all environments and only low-to-moderate overdensities, respectively.

Stellar Mass	Number of galaxies	$\langle$NUV$-r\rangle$	γ [Gyr^{-1}]
10.6<log(M$_\star$[M$_\odot$])<10.8	303	3.91	3.98±0.09
10.8<log(M$_\star$[M$_\odot$])<11.0	209	4.06	3.45±0.06
11.0<log(M$_\star$[M$_\odot$])<11.2	84	4.16	3.8±0.17

Table 5.1: Number of galaxies, median color values and quenching index in each stellar mass bin for non-AGN zCOSMOS green valley galaxies regardless of environment.

Stellar Mass	Number of galaxies	$\langle$ NUV$-r\rangle$	γ [Gyr^{-1}]
10.6<log(M$_\star$[M$_\odot$])<10.8	16	4.11	5.08±0.64
10.8<log(M$_\star$[M$_\odot$])<11.0	13	3.82	3.9±0.75
11.0<log(M$_\star$[M$_\odot$])<11.2	13	4.13	4.28±0.75

Table 5.2: Number of galaxies, median color values and quenching index in each stellar mass bin for AGN zCOSMOS green valley galaxies regardless of environment.

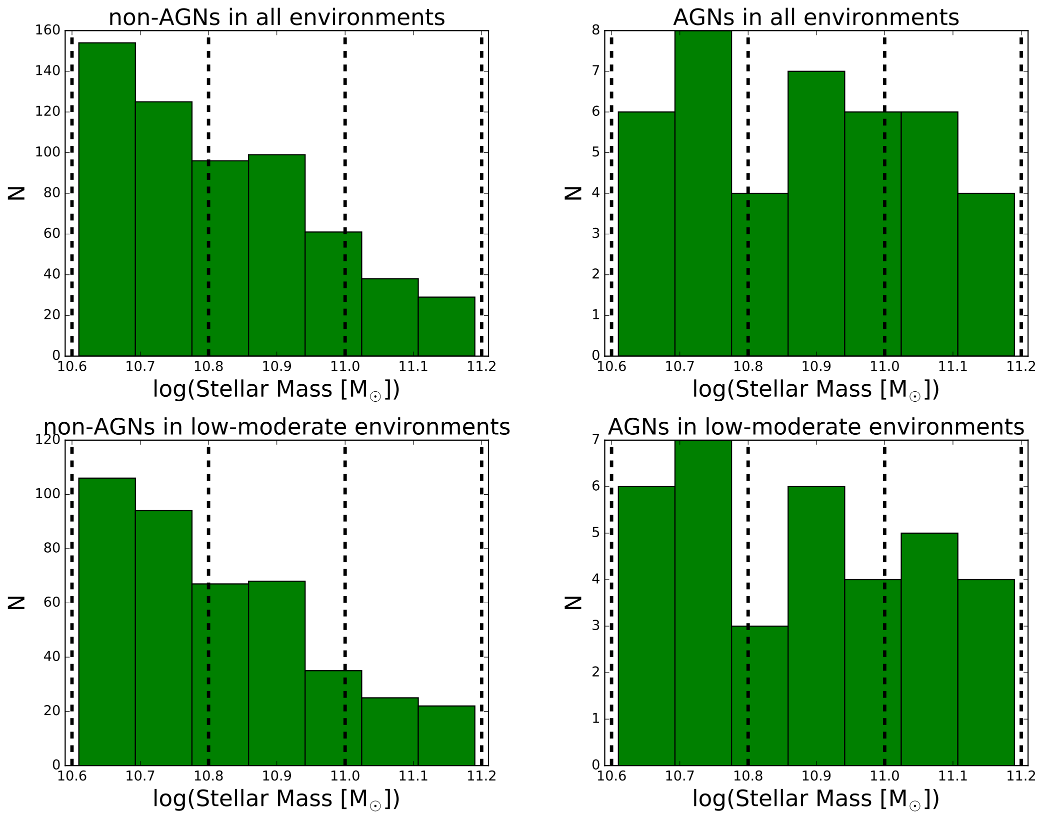

Figure 5.1: Stellar mass distribution for AGN and non-AGN green valley galaxies from our sample regardless of environment (top) and excluding galaxies in high-density environments (bottom). The vertical dashed black lines delimit the stellar mass bins in each distribution.

Stellar Mass	Number of galaxies	$\langle$NUV$-r\rangle$	γ [Gyr^{-1}]
$10.6<\log(M_\star[M_\odot])<10.8$	213	3.89	3.72 ± 0.09
$10.8<\log(M_\star[M_\odot])<11.0$	142	4.01	3.5 ± 0.08
$11.0<\log(M_\star[M_\odot])<11.2$	53	4.19	3.95 ± 0.26

Table 5.3: Number of galaxies, median color values and quenching index in each stellar mass bin for non-AGN zCOSMOS green valley galaxies in environments with low-to-moderate galaxy number overdensities.

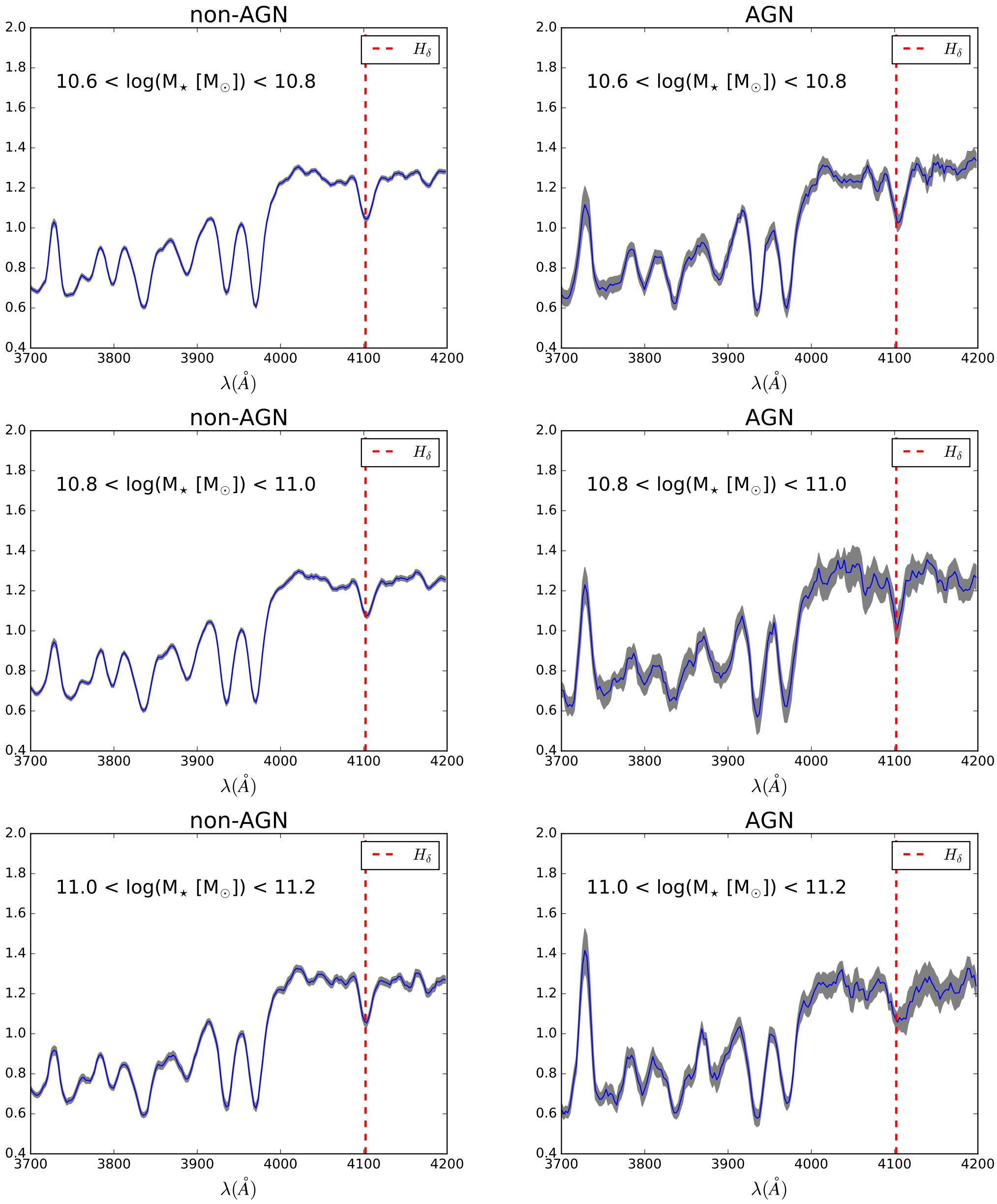

Figure 5.2: Coadded spectra of the zCOSMOS galaxy samples (blue lines) for three different stellar mass bins, regardless of environment. The left panels correspond to non-AGN green valley galaxies and the right panels to AGN counterparts. The gray region represents the standard deviation in each pixel. The y-axes are in units of erg cm^{-2} s^{-1} Å^{-1}.

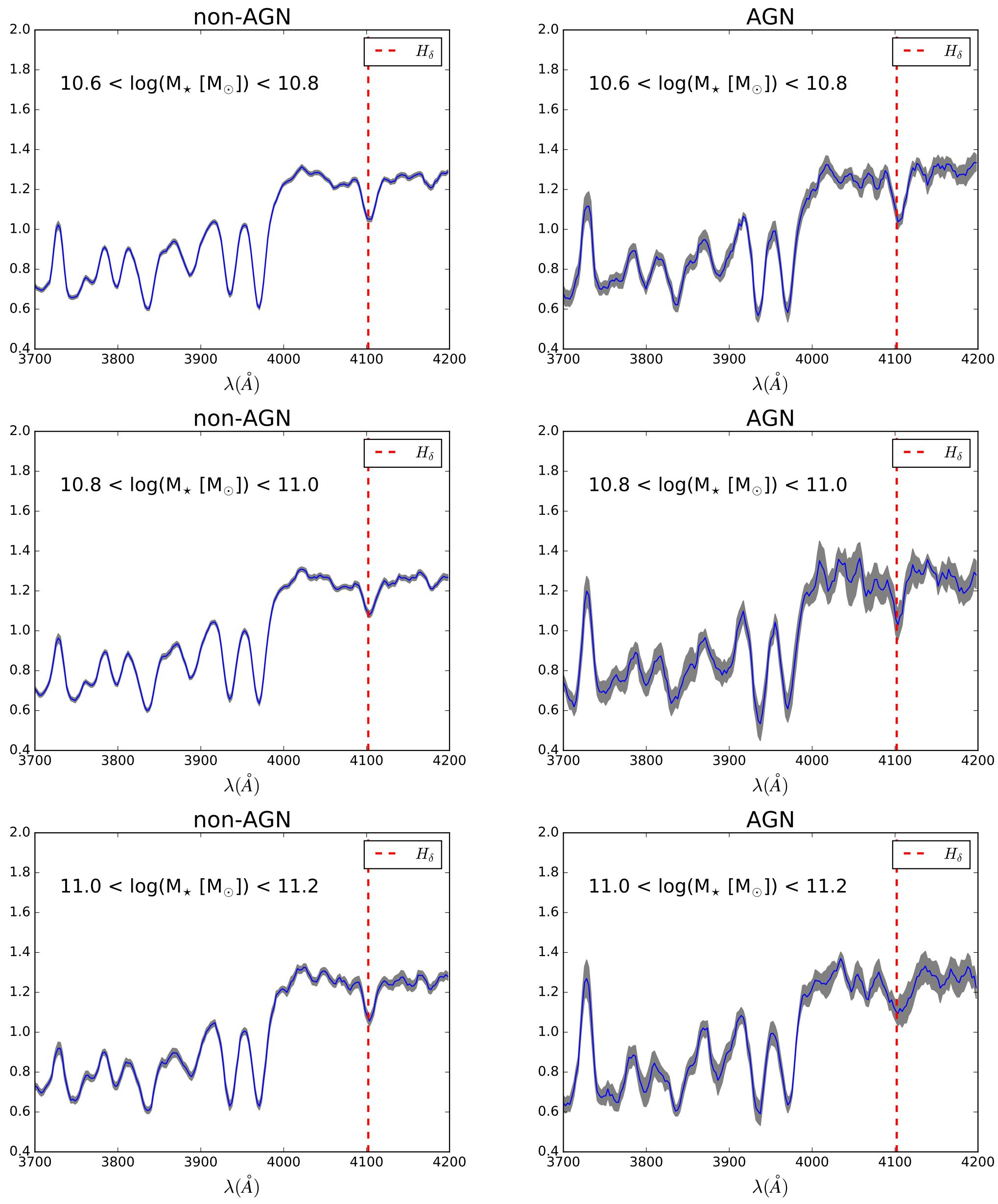

Figure 5.3: Same as Figure 5.2, but excluding galaxies in high overdensity environments

Stellar Mass	Number of galaxies	$\langle$NUV$-r\rangle$	γ [Gyr^{-1}]
$10.6<\log(M_\star[M_\odot])<10.8$	14	4.11	4.28±0.43
$10.8<\log(M_\star[M_\odot])<11.0$	11	4.13	4.56±0.97
$11.0<\log(M_\star[M_\odot])<11.2$	10	4.21	6.91±2.08

Table 5.4: Number of galaxies, median color values and quenching index in each stellar mass bin for AGN zCOSMOS green valley galaxies in environments with low-to-moderate galaxy number overdensities.

We determine $H_{\delta,A}$ and $D_n(4000)$ values for each of the considered coadds: (1) all AGN galaxies regardless of environment; (2) all non-AGNs regardless of environment; (3) all AGN galaxies within low-to-intermediate overdensities; and (4) all non-AGN galaxies within low-to-intermediate overdensities. Figures 5.4 and 5.5 show these results within their specific $H_\delta - D_n(4000)$ diagram, where SFH curves are shown for a given NUV$-r$ color, corresponding to the average color of the galaxies composing the coadded spectrum in consideration. From these results we derive star formation quenching indices and their corresponding uncertainties. These results are shown on Tables 5.1, 5.2, 5.3 and 5.4.

We investigate the evolution of the star formation quenching indices as a function of the stellar mass for non-AGN and AGN green valley galaxies (see Figure 5.6). First focusing on galaxies with an AGN (orange curves in Figure 5.6), we note that when considering all environments, we see no trend between quenching timescales and stellar mass. However, this changes when we restrict the sample to AGN galaxies found in environments with low-to-intermediate overdensities: there is a sustained increase in star formation quenching index as we consider higher mass bins $-$ that is, more massive green valley galaxies with an AGN in low-moderate environments will quench more rapidly than low-mass AGN galaxies. Comparing with our control sample of galaxies with no AGN signatures at the wavebands considered (i.e., X-ray, mid-IR and radio), we see that at the highest-mass bin galaxies with an AGN appear to quench faster than their non-AGN counterparts. However, the difference in quenching timescales between AGNs and non-AGNs of the higher masses is only detected when high-density environments are excluded, suggesting that the

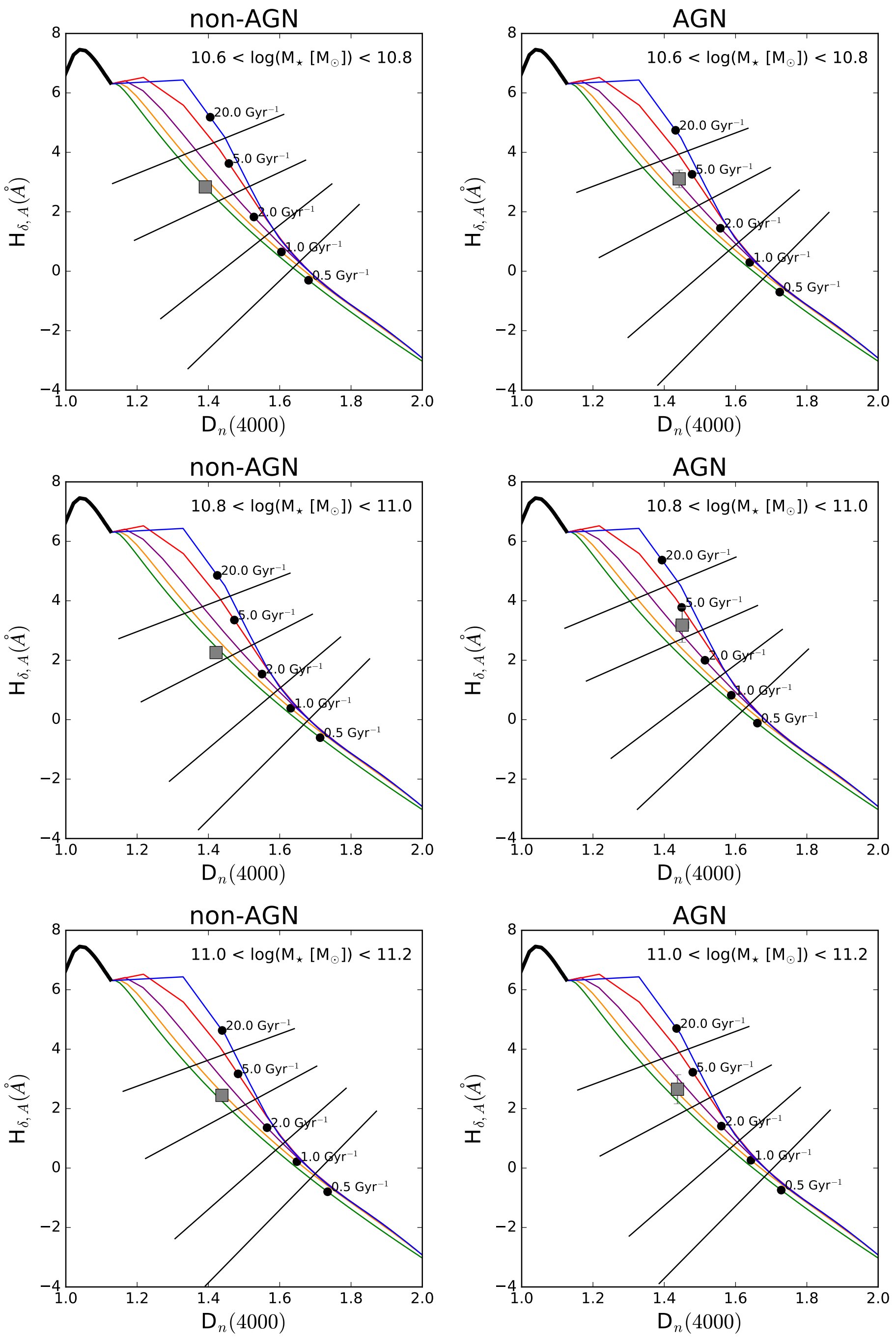

Figure 5.4: $H_{\delta,A}\times$ $D_n(4000)$ diagrams with measured indices for non-AGN (left panels) and AGN (right panels) coadds, including all galaxies regardless of environment, separated into three stellar mass intervals. The black dots represent the $D_n(4000)$ and $H_{\delta,A}$ values in each SFH model for the given NUV$-r$, which corresponds to the average NUV$-r$ color of the galaxies in each coadd. The error is the standard deviation of the indices. The straight lines represent the geometric mean in two consecutive SFH models.

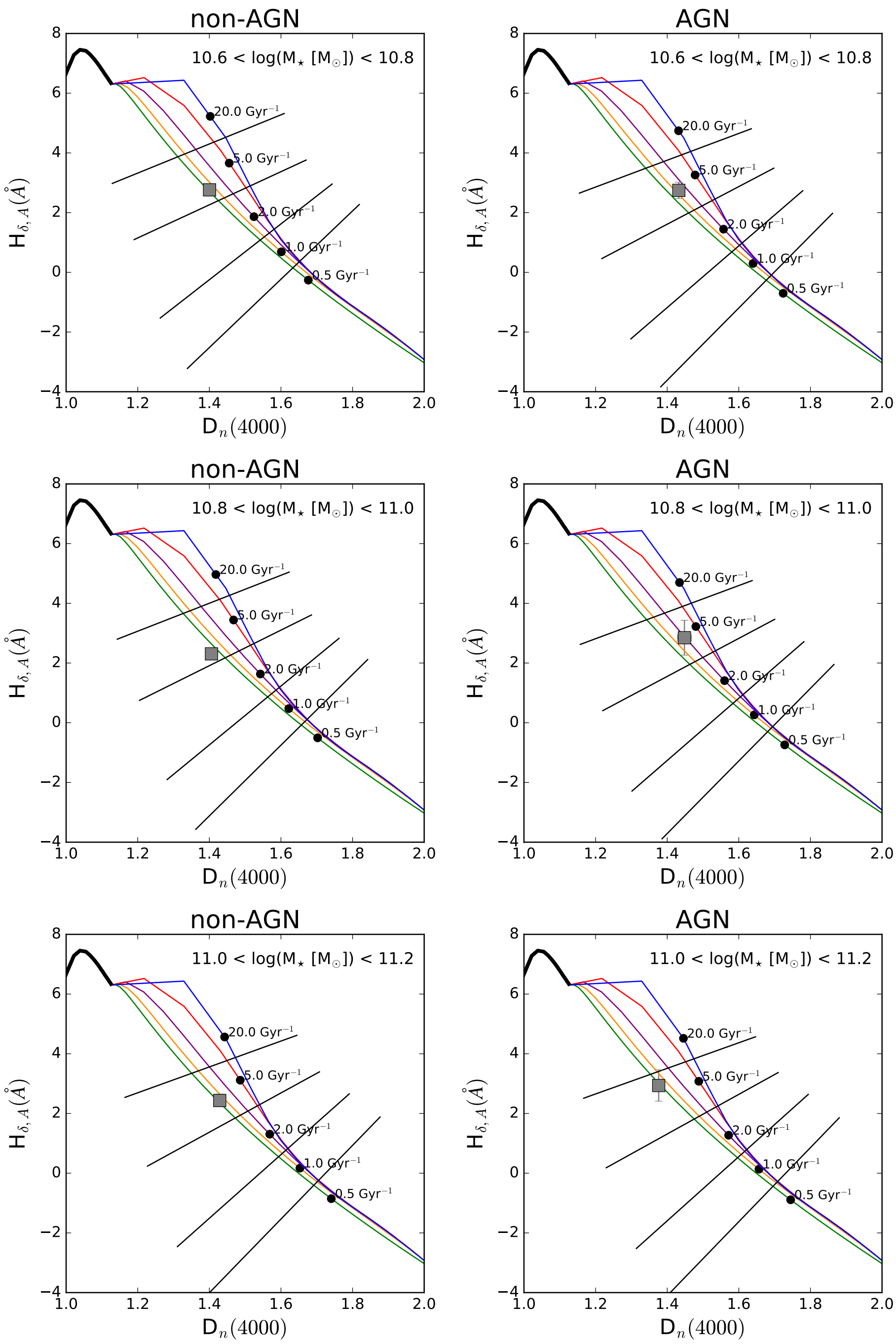

Figure 5.5: Same as Figure 5.4, but considering coadds built from green valley galaxies in low-to-intermediate overdensity environments

environment exerts an important effect that ultimately may mask the impact of an AGN within the context of star formation quenching.

We note that, although no trend with stellar mass is observed for the quenching timescales in AGN galaxies in all environments (left panel Figure 5.6), our analysis for the lowest-mass bin points to a higher quenching timescale for AGN galaxies when compared to non-AGN. As we exclude galaxies in high-density environments, the quenching timescales for the non-AGN galaxies are relatively undisturbed considering the measurement uncertainties, with the exception of the lowest stellar mass bin, where γ drops from 3.98 ± 0.09 to 3.72 ± 0.09. For the AGN sample the main changes happen in the lowest and highest mass bins; the γ index in the former drops in value and the later increases more significantly. However, these changes are all within the measurement uncertainties, which are driven by the low numbers in the case of the AGN sample. A larger sample of AGNs would likely allow us to better address the independent effects of the AGN and environment.

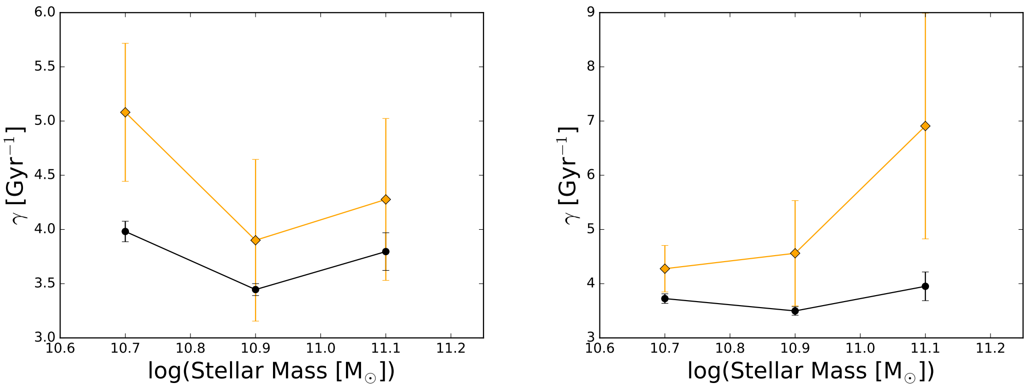

Figure 5.6: Star formation quenching index (γ) values for the non-AGN (black) and AGN (orange) green valley galaxies as a function of stellar mass in all environments (left) and in low-moderate environments (right).

5.4 Discussion

To test the robustness of our results obtained with coadded spectra from zCOSMOS we do the same analysis using spectra for individual galaxies from the LEGA-C survey. The great advantage of using LEGA-C is that individual galaxy spectra have enough S/N to calculate the spectral indices $D_n(4000)$ and $H_{\delta,A}$ for individual green valley galaxies. Although the star formation indices derived for our coadds are expected to be more representative of the general population, these individual spectra from LEGA-C allow us to explore in a more independent manner a number of additional factors that may impact quenching in these galaxies.

We identified 6 AGNs in the LEGA-C dataset within the stellar mass range considered for our analysis and with adequate optical spectra[1]. We note that 2 of these lie in high-density environment and are thus excluded in our discussion of galaxies in environments within low-to-intermediate overdensities. We derive star formation quenching indices for all 6 galaxies and compare the range of values covered with the typical values derived for our coadds. The comparison of quenching indices obtained for zCOSMOS and LEGA-C are shown in Figure 5.7.

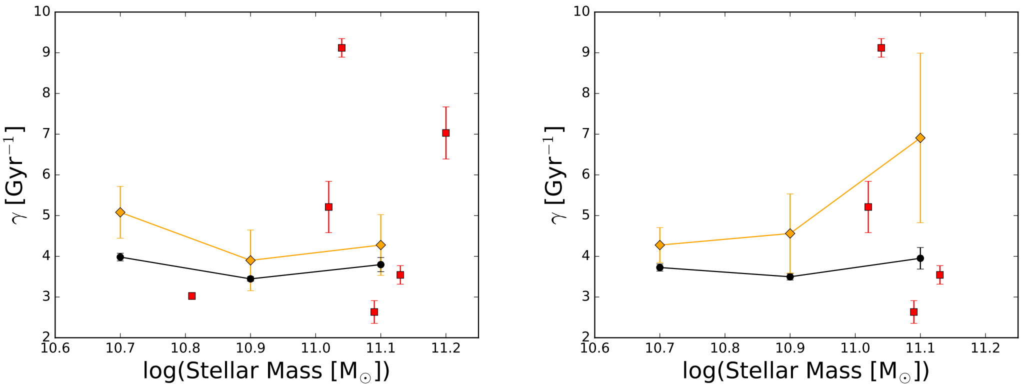

Figure 5.7: Same as Figure 5.6, but including datapoints from our analysis on the LEGA-C individual galaxies (red squares).

The star formation quenching indices derived for the individual LEGA-C points in Figure 5.7 cover a broad range of values, which we attribute for the most part to differences in morphology. Half of all LEGA-C AGNs are classified as disks (see Table 5.5) by the ZEST morphological catalog and confirmed by visual inspection; these correspond to the LEGA-C AGNs with the lowest γ values derived (see Figure 5.7). Considering our findings from Chapter 3, we attribute the longer quenching timescales to their disk-like morphology. On the other hand, two out

[1]We eliminated from our analysis one LEGA-C AGN with a spectral artifact coinciding with the $H_{\delta,A}$ absorption, which made a calculation of the $H_{\delta,A}$ index impossible.

of the 3 LEGA-C AGNs with higher γ values are associated with spheroidal morphologies. This distribution in morphology as a function of γ values is consistent with our findings on Chapter 3. The only exception is the LEGA-C AGN with the highest derived gamma value − although identified as a disk, this AGN is identified as a radio-loud AGN which likely drives the star formation quenching index up in association with a more extreme phase of AGN feedback and thus, faster quenching.

Environment	Disk (fraction)	Elliptical (fraction)	Others (fraction)
All	0.5	0.5	0.0
Low-moderate	0.5	0.5	0.0

Table 5.5: Distribution of morphologies for the sample of AGN green valley galaxies in the LEGA-C survey.

We note that the general morphological composition of our zCOSMOS coadds (shown on Tables 5.6 and 5.7) is dominated by disks. The morphological composition of the AGN coadd in the highest mass bin (excluding high density environments) is slightly different, considering that morphologies associated with faster quenching (ellipticals, irregulars and mergers; see Chapter 3) make up half of the galaxies that go into the coadd (see Table 5.7). Following the same arguments used to understand the gamma values for the LEGA-C AGNs, this suggests that the increase in gamma values for the highest mass bin may be a combined result of morphology and AGN content.

Stellar Mass	Disk (fraction)	Elliptical (fraction)	Others (fraction)
$10.6<\log(M_\star[M_\odot])<10.8$	0.69	0.25	0.06
$10.8<\log(M_\star[M_\odot])<11.0$	0.64	0.36	0.0
$11.0<\log(M_\star[M_\odot])<11.2$	0.6	0.3	0.1

Table 5.6: Distribution of morphologies in the zCOSMOS sample of green valley galaxies regardless of their environments.

We consider the potential impact that different AGN selection methods may have in the AGN population probed by our zCOSMOS coadd-based results and those of the LEGA-C AGN sample. However, we verified that the relative proportions of

Stellar Mass	Disk (fraction)	Elliptical (fraction)	Others (fraction)
$10.6<\log(M_\star[M_\odot])<10.8$	0.64	0.36	0.0
$10.8<\log(M_\star[M_\odot])<11.0$	0.73	0.27	0.0
$11.0<\log(M_\star[M_\odot])<11.2$	0.5	0.4	0.1

Table 5.7: Distribution of morphologies in the zCOSMOS sample of green valley galaxies within environments of low-to-moderate overdensities.

green valley AGNs detected in X-ray (Chandra and/or XMM-Newton), mid-infrared (Spitzer) and radio (VLA) bands in our zCOSMOS sample reveal a similarly-mixed composition as that of the LEGA-C AGN sample we use (see Tables 5.8, 5.9 and 5.10).

Environment	X-ray (fraction)	Infrared (fraction)	Radio (fraction)
All	0.5	0.33	0.17
Low-moderate	0.5	0.25	0.25

Table 5.8: Fraction of AGN green valley galaxies in LEGA-C survey detected in each at each waveband.

Stellar Mass	X-ray (fraction)	Infrared (fraction)	Radio (fraction)
$10.6<\log(M_\star[M_\odot])<10.8$	0.81	0.06	0.13
$10.8<\log(M_\star[M_\odot])<11.0$	0.46	0.15	0.38
$11.0<\log(M_\star[M_\odot])<11.2$	0.62	0.23	0.38

Table 5.9: Fraction of AGN green valley galaxies in zCOSMOS survey (regardless of their environment), detected iat each waveband.

We do find a potential difference in the NUV$-r$ color distribution of the populations probed by the zCOSMOS sample of AGNs and that of LEGA-C (see Figure 5.8). Although the distributions are not strikingly different, the zCOSMOS sample appears to extend towards higher NUV$-r$ values, i.e., the zCOSMOS has a higher number of redder galaxies. At this stage, work is still underway to explore the impact that these differences may have in our comparison between LEGA-C

Stellar Mass	X-ray (fraction)	Infrared (fraction)	Radio (fraction)
$10.6<\log(M_\star[M_\odot])<10.8$	0.79	0.07	0.14
$10.8<\log(M_\star[M_\odot])<11.0$	0.55	0.09	0.36
$11.0<\log(M_\star[M_\odot])<11.2$	0.5	0.3	0.4

Table 5.10: Fraction of AGN green valley galaxies (within environments of low-to-moderate overdensities) in our zCOSMOS sample detected at each waveband.

individual quenching timescales and those of our coadds. Moreover, we are in the process of exploring a number of other lines of investigation, including the dependence of quenching timescales on redshift and on NUV$-r$ color within the green valley.

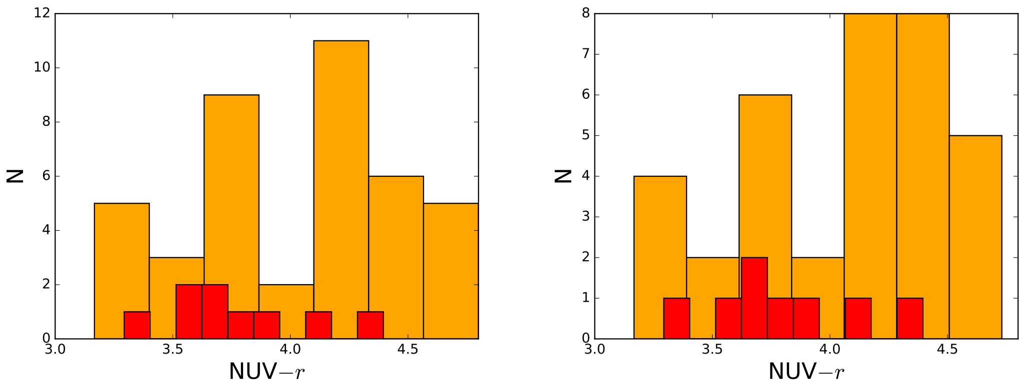

Figure 5.8: NUV$-r$ color distribution in all environments (left) and for low-moderate overdensity environments (right). The orange distributions represent zCOSMOS green valley galaxies and the red distributions represent the LEGA-C ones.

We assess the evolution of the AGN fraction in green valley galaxies with their stellar mass (Figure 5.9) and note that the AGN fraction increases with stellar mass. This not only is consistent with earlier works that point to the presence of AGN in massive galaxies (e.g., Di Matteo et al., 2005), but also fits into a coherent picture with our own results that AGN activity is more important in more massive green valley galaxies. We furthermore study the AGN fraction in our sample as a function of NUV$-r$ color and identify an increase as we move from the blue cloud onto the green valley. This observation is consistent with the peak in the AGN fraction that has been identified in the green valley by earlier works (Nandra et al., 2007; Martin et al., 2007; Hickox et al., 2009; Schawinski et al., 2010). Considering the combination of these results − an increase in AGN fraction within the green valley, an increase in AGN fraction for more massive galaxies and a shorter quenching timescale for more massive AGN hosts − we conclude that AGNs play an important role in the passage of galaxies from the blue cloud to the red sequence (see also Smethurst et al., 2016).

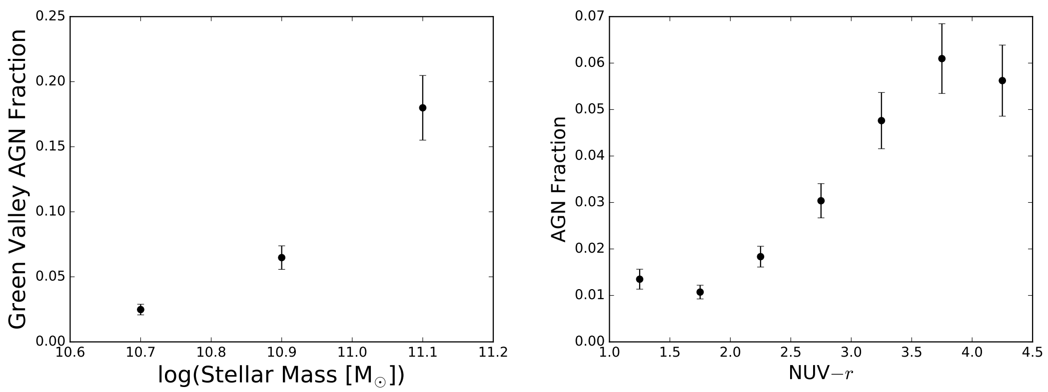

Figure 5.9: ***Left:*** Evolution of the green valley AGN fraction as a function of stellar mass. ***Right:*** Evolution of AGN fraction as a function of NUV−r, in equally-spaced color bins, comprising the blue cloud (NUV−r < 3.0) and the green valley (NUV−r > 3.0). We do not extent to the red sequence because the red galaxies in our sample are not well represented (Section 2.2 in Chapter 2). The error bars are calculated as $[f(1-f)/N]^{1/2}$ (Sheth et al., 2008), where f is the AGN fraction in each bin and N is the total of galaxies in each bin.

The need to consider morphology and environment to interpret our results emphasizes the difficulty in isolating the independent effects of morphology, AGN content and environment. The fact that we uncover higher star formation quenching indices (i.e., faster quenching) for high-mass galaxies with an AGN only when excluding high-density environments suggests that the environment plays a non-negligible role in quenching star formation even in the presence of an AGN; the impact of an AGN is not sufficient to rise above the effect of the environment. However, this picture changes when we consider more moderate environments. Furthermore, we are confronted with the fact that even after excluding high-density environments from our analysis the LEGA-C AGNs display a broad range of gamma values that suggest that AGN content is likely not the only factor that determines quenching fate of green valley galaxies; morphology − and the underlying processes that it represents − plays a role, too.

Chapter 6

Summary

Gas consumption in galaxies is a natural result of the star formation process and hence, of the buildup of stellar mass at all cosmic epochs. At any given epoch, galaxies in the process of forming stars typically will do so at a rate that depends on their stellar mass ($M_{\star}$). This correlation is what gives rise to the main sequence of star forming galaxies − a tight correlation recently observed between star formation rate (SFR) and stellar mass (e.g., Noeske et al., 2007). This sequence moves towards higher SFRs and higher stellar masses as we go back in redshift and has been confirmed out to $z \sim 2.5$ (e.g., Whitaker et al., 2012). The average gas consumption for main sequence star-forming galaxies is $\sim$ 2 Gyrs in the local universe (Bigiel et al., 2008) and $\sim$ 700 Myrs at $z = 3$ (Tacconi et al., 2013). These timescales are not consistent with the scarcity of galaxies within the green valley region of the color-magnitude diagram (CMD) and the observed growth of the red sequence of galaxies (Faber et al., 2007). With these timescales, the natural gas consumption caused by star formation activity as observed in the main-sequence of star-forming galaxies should in principle lead galaxies to undergo a relatively smooth color transition on the galaxy CMD. Consequently, we would not observe a galaxy bimodality. It becomes clear that other astrophysical agents must be responsible for triggering sudden episodes of intense gas exhaustion (e.g., nuclear and/or galaxy-wide starbursts) that rapidly drive the galaxy-wide color transition at a faster pace. Indeed, recent studies have shown that the average timescale for star formation quenching is much shorter than that predicted by the consumption of gas from star formation activity: $\sim$ 1 Gyr in the local universe (Martin et al., 2007); and $\sim$ 200 Myrs at

$z \sim 0.8$ (Gonçalves et al., 2012).

In order to understand the nature of the galaxy mechanisms that drive the rapid color transition through the green valley at intermediate redshifts in this Ph.D. thesis we analyze the star formation quenching timescales in green valley galaxies at $0.5 < z < 1.0$ as a function of galaxy morphology, compactness and the presence of an active galactic nucleus (AGN). To quantify the star formation quenching timescales, we adopt the same approach used by Martin et al. (2007) and Gonçalves et al. (2012), considering a simple model for the star formation history (SFH) for each galaxy: a constant star formation rate for the first $t_0 = 6$ Gyrs followed by a period of exponential decay, parametrized by the exponential index γ ($e^{-\gamma t}$). This exponential index corresponds to the star formation quenching index and can be translated into a star formation quenching timescale ($1/\gamma$ in units of Gyr) corresponding to the time when the initial star formation rate has decreased down to 37% of its initial value. We determine the value of gamma based on measuring the rest-frame 4000 Å break, the strength of the H_δ absorption line and the NUV$-r$ color of green valley galaxies. These spectral indices are sensitive to the SFH (Kauffmann et al., 2003) and the NUV$-r$ color is sensitive to the stellar population content.

Taking advantage of the wealth in multi-band photometric and spectroscopic data within the COSMOS field, we use COSMOS galaxies as a starting point for our parent sample. We use rest-frame NUV$-r$ colors from the Canada-France-Hawaii Telescope Legacy Survey (CFHTLS) to identify green valley galaxies and cross-match these with the 10k and 20k zCOSMOS spectroscopic survey (Lilly et al., 2007) to obtain individual spectra for our final sample. Relying on complementary catalogs and/or analysis regarding morphology, compactness and AGN content we determine typical star formation quenching timescales from green valley galaxies according to such properties. Although previous studies have addressed the morphological and AGN composition of green valley galaxies (i.e., green valley fraction with respect to that within the blue cloud and the red sequence; see review by Salim (2014), this is the first time that a quantitative analysis has been performed on the timescale calculation for star formation quenching as a function of galaxy properties. This thesis presents this work in the following three fronts:

- *Star formation quenching as a function of galaxy morphology*

We devise a morphological classification that divides galaxies into disks, ellipticals and irregulars (based on the Zurich Estimator of Structure Types Catalog or ZEST, Scarlata et al., 2007), subdivides disks into strongly-barred, weakly-barred and unbarred (based on the bar catalog of Sheth et al., 2008) and considers a separate "merger" category (for systems with tidal tails pointing to interactions between multiple galaxies). Following this morphological classification, we find that disks have longer star formation quenching timescales than ellipticals, irregulars and mergers, suggesting that intense processes − with which the latter morphologies are typically associated − are more efficient at winding down star formation activity in their host galaxies than disks. In particular, we find that systems in the midsts of a merger typically quench their star formation 5 times faster than undisturbed disks. Contrastingly, barred galaxies display the lowest star formation quenching timescales among all galaxy types, suggesting that these are sites where no other major quenching external agents have had an impact as they transition through the green valley.

- *Star formation quenching as a function of galaxy compactness*

  In an effort to study star formation quenching in galaxies that give rise to compact, massive, passive galaxies (baptized as red nuggets) that still baffle galaxy formation models, we identify the so-called green nuggets and calculate their rate of passage through the green valley. We divide our sample of green valley galaxies into ultra-compact, compact and normal-sized galaxies based on the stellar masses provided by the UltraVISTA catalog and angular sizes of the ZEST catalog. Excluding objects residing in significant overdensities, we find that the star formation quenching timescales in green nuggets (ultra-compact and compact galaxies) are $2 - 5$ times shorter than in normal-sized galaxies. These results are consistent with scenarios of violent disk instability that can cause a rapid transition from a compact star-forming galaxy (blue nugget) to a passive compact one (red nugget) in the presence of high gas fractions (e.g., Dekel & Burkert, 2014). The decrease in typical gas content in galaxies with cosmic times suggests that this scenario becomes much less common at $z < 1$, which reflects in the low number of green nuggets at these redshifts.

- *Star formation quenching as a function of AGN presence*

  Feedback from an AGN has been one of the favorite candidates to explain the rapid passage of galaxies through the green valley. On the one hand low-z studies point to an increase in the AGN fraction in green valley galaxies compared to the blue cloud and the red sequence (e.g., Martin et al., 2007); on the other hand, studies have pointed to differences in the AGN and the green valley timescales, suggesting that such a connection is not trivial. For the first time, we undertook the quantification of star formation quenching timescales in green valley galaxies with and without an AGN in order to compare the relative pace with which they traverse the green valley. For this we identify AGNs based on X-ray, mid-infrared and radio band selection. Once limited to galaxies in environments with low-to-moderate overdensities, we find that massive (log $M_\star \sim 11 - 11.2$) green valley galaxies hosting an AGN quench their star formation almost twice as fast as non-AGN green valley galaxies of the same mass.

Our analysis of star formation quenching timescales as a function of galaxy morphology, compactness and the presence of AGN at intermediate redshifts ($z \sim 0.5 - 1$) suggests a quenching scenario where a mixture of astrophysical processes are at play. Both slow processes, in the form of secular evolution (spiral arms and bars), and fast processes, in the form of mergers, violent disk instability and AGN feedback are very common within the green valley. Therefore, in the general context of star formation quenching, our results in this Ph.D thesis suggest that the cessation of star formation follows different evolutionary paths on the color-magnitude-diagram.

Although disk galaxies are relatively common in the green valley ($\sim 30\%$) at the intermediate redshifts studied in this thesis, they do not appear to play a important role in quenching star formation in green valley galaxies. Faster mechanisms, like galaxy interaction (associated with the elliptical, irregular and merger morphologies) and AGN feedback contribute, to a more significant degree, to the transition of galaxies through the green valley at $0.5 < z < 1.0$. Violent disk instability does have an important impact in the color transition of massive compact green valley galaxies, however because this subpopulation of galaxies is not as abundant within the green valley, this process contributes in a smaller proportion to the color transition of the general galaxy population at intermediate redshifts.

When we turn our attention to green valley galaxies within the local universe, the majority are disks (Schawinski et al., 2014; Salim, 2014). Although many of these galaxies host an AGN (Martin et al., 2007), the observed predominance of disks and the typical quenching timescale 5 times slower than at $z \sim 0.8$, suggests that the green valley in the local universe may have a stronger contribution from secular evolution. This in turn provides an explanation as to why star formation quenching happens at a faster pace at $z \sim 0.8$. The observed increase in merger and AGN activity at higher redshifts, as well as the expected increase in violent disk instability as a result of an increase in gas content in galaxies optimizes conditions for green valley galaxies to efficiently quench their star formation at a faster rate than would be possible with agents of secular evolution. At these intermediate redshifts, green valley galaxies appear to be undergoing a global color transformation due to a higher incidence of these intense processes that in turn lead to a faster migration through the green valley in the color-magnitude diagram of the general galaxy population.

Bibliography

Aird J., et al., 2010, MNRAS, 401, 2531

Alongi M., Bertelli G., Bressan A., Chiosi C., Fagotto F., Greggio L., Nasi E., 1993, A&AS, 97, 851

Athanassoula E., Machado R. E. G., Rodionov S. A., 2013, MNRAS, 429, 1949

Baldry I. K., Glazebrook K., Brinkmann J., Ivezić Ž., Lupton R. H., Nichol R. C., Szalay A. S., 2004, ApJ, 600, 681

Baldry I. K., Balogh M. L., Bower R. G., Glazebrook K., Nichol R. C., Bamford S. P., Budavari T., 2006, MNRAS, 373, 469

Baldry I. K., Glazebrook K., Driver S. P., 2008, MNRAS, 388, 945

Baldwin J. A., Phillips M. M., Terlevich R., 1981, PASP, 93, 5

Balogh M. L., Morris S. L., Yee H. K. C., Carlberg R. G., Ellingson E., 1999, ApJ, 527, 54

Balogh M. L., Baldry I. K., Nichol R., Miller C., Bower R., Glazebrook K., 2004, ApJ, 615, L101

Barro G., et al., 2013, ApJ, 765, 104

Barro G., et al., 2015, preprint, (arXiv:1509.00469)

Behroozi P. S., Wechsler R. H., Conroy C., 2013, ApJ, 770, 57

Bertoldi F., et al., 2007, ApJS, 172, 132

Bigiel F., Leroy A., Walter F., Brinks E., de Blok W. J. G., Madore B., Thornley M. D., 2008, AJ, 136, 2846

Blanton M. R., Roweis S., 2007, AJ, 133, 734

Bournaud F., Elmegreen B. G., Elmegreen D. M., 2007, ApJ, 670, 237

Bournaud F., Daddi E., Weiß A., Renaud F., Mastropietro C., Teyssier R., 2015, A&A, 575, A56

Bressan A., Fagotto F., Bertelli G., Chiosi C., 1993, A&AS, 100, 647

Bruzual G., Charlot S., 2003, MNRAS, 344, 1000

Bundy K., et al., 2006, ApJ, 651, 120

Calzetti D., Armus L., Bohlin R. C., Kinney A. L., Koornneef J., Storchi-Bergmann T., 2000, ApJ, 533, 682

Capak P., et al., 2007, ApJS, 172, 99

Cappelluti N., et al., 2009, A&A, 497, 635

Carollo C. M., et al., 2013, ApJ, 773, 112

Cattaneo A., et al., 2009, Nature, 460, 213

Ceverino D., Dekel A., Bournaud F., 2010, MNRAS, 404, 2151

Ceverino D., Dekel A., Mandelker N., Bournaud F., Burkert A., Genzel R., Primack J., 2012, MNRAS, 420, 3490

Chabrier G., 2003, ApJ, 586, L133

Charbonnier A., et al., 2017, MNRAS, 469, 4523

Cheung E., et al., 2012, ApJ, 760, 131

Ciotti L., Ostriker J. P., 2007, ApJ, 665, 1038

Civano F., et al., 2016, ApJ, 819, 62

Coil A. L., et al., 2008, ApJ, 672, 153

Conselice C. J., 2006, ApJ, 638, 686

Conselice C. J., Chapman S. C., Windhorst R. A., 2003, ApJ, 596, L5

Cowie L. L., Songaila A., Hu E. M., Cohen J. G., 1996, AJ, 112, 839

Croton D. J., et al., 2006, MNRAS, 365, 11

Damjanov I., et al., 2011, ApJ, 739, L44

Darvish B., Sobral D., Mobasher B., Scoville N. Z., Best P., Sales L. V., Smail I., 2014, ApJ, 796, 51

Darvish B., Mobasher B., Sobral D., Scoville N., Aragon-Calvo M., 2015, ApJ, 805, 121

Darvish B., Mobasher B., Sobral D., Rettura A., Scoville N., Faisst A., Capak P., 2016, ApJ, 825, 113

Dekel A., Birnboim Y., 2006, MNRAS, 368, 2

Dekel A., Burkert A., 2014, MNRAS, 438, 1870

Dekel A., Devor J., Hetzroni G., 2003, MNRAS, 341, 326

Delgado-Serrano R., Hammer F., Yang Y. B., Puech M., Flores H., Rodrigues M., 2010, A&A, 509, A78

Di Matteo T., Springel V., Hernquist L., 2005, Nature, 433, 604

Dubois Y., Gavazzi R., Peirani S., Silk J., 2013, MNRAS, 433, 3297

Faber S. M., et al., 2007, ApJ, 665, 265

Fagotto F., Bressan A., Bertelli G., Chiosi C., 1994b, A&AS, 105

Fagotto F., Bressan A., Bertelli G., Chiosi C., 1994a, A&AS, 105

Fang J. J., Faber S. M., Koo D. C., Dekel A., 2013, ApJ, 776, 63

Farouki R., Shapiro S. L., 1981, ApJ, 243, 32

Ferrarese L., Merritt D., 2000, ApJ, 539, L9

Furlong M., et al., 2017, MNRAS, 465, 722

Gebhardt K., et al., 2000, ApJ, 539, L13

Genzel R., et al., 2010, MNRAS, 407, 2091

Gonçalves T. S., Martin D. C., Menéndez-Delmestre K., Wyder T. K., Koekemoer A., 2012, ApJ, 759, 67

Graham A. W., Scott N., 2013, ApJ, 764, 151

Griffith R. L., Stern D., 2010, AJ, 140, 533

Gültekin K., et al., 2009, ApJ, 698, 198

Gunn J. E., Gott III J. R., 1972, ApJ, 176, 1

Häring N., Rix H.-W., 2004, ApJ, 604, L89

Hasinger G., et al., 2007, ApJS, 172, 29

Hickox R. C., et al., 2009, ApJ, 696, 891

Ho L. C., Filippenko A. V., Sargent W. L. W., 1997, ApJ, 487, 591

Hubble E. P., 1926, ApJ, 64

Ilbert O., et al., 2013, A&A, 556, A55

Juneau S., et al., 2005, ApJ, 619, L135

Kauffmann G., et al., 2003, MNRAS, 341, 33

Kennicutt Jr. R. C., 1998, ApJ, 498, 541

Kormendy J., Bender R., 1996, ApJ, 464, L119

Kormendy J., Kennicutt Jr. R. C., 2004, ARA&A, 42, 603

Kriek M., van Dokkum P. G., Franx M., Illingworth G. D., Magee D. K., 2009, ApJ, 705, L71

Lagos C. d. P., Lacey C. G., Baugh C. M., 2013, MNRAS, 436, 1787

Larson R. B., Tinsley B. M., Caldwell C. N., 1980, ApJ, 237, 692

Lilly S. J., et al., 2007, ApJS, 172, 70

Lotz J. M., Jonsson P., Cox T. J., Croton D., Primack J. R., Somerville R. S., Stewart K., 2011, ApJ, 742, 103

Magorrian J., et al., 1998, AJ, 115, 2285

Marchesi S., et al., 2016, ApJ, 830, 100

Martig M., Bournaud F., Teyssier R., Dekel A., 2009, ApJ, 707, 250

Martin D. C., et al., 2005, ApJ, 619, L1

Martin D. C., et al., 2007, ApJS, 173, 342

McCracken H. J., et al., 2012, A&A, 544, A156

Mendez A. J., Coil A. L., Lotz J., Salim S., Moustakas J., Simard L., 2011, ApJ, 736, 110

Menéndez-Delmestre K., Sheth K., Schinnerer E., Jarrett T. H., Scoville N. Z., 2007, ApJ, 657, 790

Moore B., Lake G., Katz N., 1998, ApJ, 495, 139

Murray N., Quataert E., Thompson T. A., 2005, ApJ, 618, 569

Naab T., Johansson P. H., Ostriker J. P., 2009, ApJ, 699, L178

Nandra K., et al., 2007, ApJ, 660, L11

Noeske K. G., et al., 2007, ApJ, 660, L43

Pan Z., Kong X., Fan L., 2013, ApJ, 776, 14

Peng Y.-j., et al., 2010, ApJ, 721, 193

Puech M., 2010, MNRAS, 406, 535

Quilis V., Trujillo I., 2013, ApJ, 773, L8

Salim S., 2014, Serbian Astronomical Journal, 189, 1

Salim S., et al., 2007, ApJS, 173, 267

Salim S., et al., 2009, ApJ, 700, 161

Sandage A., 1961, The Hubble atlas of galaxies

Sanders D. B., et al., 2007, ApJS, 172, 86

Sargent M. T., et al., 2007, ApJS, 172, 434

Scarlata C., et al., 2007, ApJS, 172, 406

Schawinski K., et al., 2009, ApJ, 690, 1672

Schawinski K., et al., 2010, ApJ, 711, 284

Schawinski K., et al., 2014, MNRAS, 440, 889

Schinnerer E., et al., 2007, ApJS, 172, 46

Schmidt M., 1959, ApJ, 129, 243

Scoville N., et al., 2007, ApJS, 172, 1

Sheth K., Vogel S. N., Regan M. W., Thornley M. D., Teuben P. J., 2005, ApJ, 632, 217

Sheth K., et al., 2008, ApJ, 675, 1141

Sheth K., Melbourne J., Elmegreen D. M., Elmegreen B. G., Athanassoula E., Abraham R. G., Weiner B. J., 2012, ApJ, 758, 136

Sijacki D., Springel V., 2006, MNRAS, 366, 397

Smethurst R. J., et al., 2016, MNRAS, 463, 2986

Spitzer Jr. L., Schwarzschild M., 1951, ApJ, 114, 385

Spitzer Jr. L., Schwarzschild M., 1953, ApJ, 118, 106

Springel V., Di Matteo T., Hernquist L., 2005, MNRAS, 361, 776

Stoughton C., et al., 2002, AJ, 123, 485

Strateva I., et al., 2001, AJ, 122, 1861

Tacconi L. J., et al., 2010, Nature, 463, 781

Tacconi L. J., et al., 2013, ApJ, 768, 74

Toomre A., 1977, in Tinsley B. M., Larson D. Campbell R. B. G., eds, Evolution of Galaxies and Stellar Populations. p. 401

Tremaine S., et al., 2002, ApJ, 574, 740

Wellons S., et al., 2016, MNRAS, 456, 1030

Whitaker K. E., Kriek M., van Dokkum P. G., Bezanson R., Brammer G., Franx M., Labbé I., 2012, ApJ, 745, 179

Worthey G., Ottaviani D. L., 1997, ApJS, 111, 377

Wyder T. K., et al., 2007, ApJS, 173, 293

Zamojski M. A., et al., 2007, ApJS, 172, 468

Zolotov A., et al., 2015, MNRAS, 450, 2327

de Vaucouleurs G., 1959, Handbuch der Physik, 53, 275

van Dokkum P. G., et al., 2015, ApJ, 813, 23

van der Wel A., et al., 2014, ApJ, 788, 28

van der Wel A., et al., 2016, ApJS, 223, 29

Appendix A

Estimating the Required S/N to Measure the Spectral Indices

Consider R as a function of n variables, i.e., $R = R(a_1, a_2, a_3, ..., a_n.)$. The error σ_R of the function R is given by the general equation:

$$\sigma_R = \sqrt{\left(\frac{\partial R}{\partial a_1}\right)^2 \sigma_{a_1}^2 + \left(\frac{\partial R}{\partial a_2}\right)^2 \sigma_{a_2}^2 + \ldots + \left(\frac{\partial R}{\partial a_n}\right)^2 \sigma_{a_n}^2} \ . \tag{A.1}$$

We use the above general equation to estimate the required S/N to measure the spectral indices within determined uncertainties, as shown in the next sections.

A.1 H_δ absorption line

The H_δ absorption line ($\mathrm{H}_{\delta,A}$) is defined as follows (Equation 2.4):

$$\mathrm{H}_{\delta,A} = \sum_{\lambda=4083.5}^{4122.25} \left(1 - \frac{F_\lambda}{F_{\lambda,cont}}\right) d\lambda \ . \tag{A.2}$$

The partial derivative of the above equation with respect to F_λ is:

$$\frac{\partial \mathrm{H}_{\delta,A}}{\partial F_\lambda} = \sum_{\lambda=4083.5}^{4122.25} -\frac{d\lambda}{F_{\lambda,cont}} \ . \tag{A.3}$$

Therefore, the error $\sigma_{H_{\delta,a}}$ of $\mathrm{H}_{\delta,A}$ is:

$$\sigma_{\mathrm{H}_{\delta,a}}^2 = \sum_{\lambda=4083.5}^{4122.25} \left(-\frac{d\lambda}{F_{\lambda,cont}} \sigma_{F_\lambda}\right)^2 \ . \tag{A.4}$$

We can consider the ratio $F_{\lambda,cont}/\sigma_{F_\lambda}$ as the signal-to-noise ratio (S/N). Replacing this in the equation above, we have:

$$\sigma_{\mathrm{H}_{\delta,a}} = \sqrt{\sum_{\lambda=4083.5}^{4122.25} \left(\frac{d\lambda}{S/N}\right)^2} \Rightarrow \sigma_{\mathrm{H}_{\delta,a}} = \sqrt{n}\frac{d\lambda}{S/N} \ , \tag{A.5}$$

where n is the number of elements. Considering a maximum error of $\sigma_{\mathrm{H}_{\delta,a}} = 1.5$, the minimum S/N required to properly measure the $\mathrm{H}_{\delta,A}$ index is:

$$S/N = \sqrt{n}\frac{d\lambda}{\sigma_{\mathrm{H}_{\delta,a}}} = \sqrt{38.75}\frac{1}{1.5} \sim 4 \ . \tag{A.6}$$

A.2 4000 Å break

The $\mathrm{D}_n(4000)$ index is given by (Equation 2.3):

$$\mathrm{D}_n(4000) = \sum_{\lambda=4000\text{Å}}^{4100\text{Å}} F_\lambda \Bigg/ \sum_{\lambda=3850\text{Å}}^{3950\text{Å}} F_\lambda \ . \tag{A.7}$$

We can call the upper part of the fraction in the above equation as A and the bottom part as B:

$$A = \sum_{\lambda=4000\text{Å}}^{4100\text{Å}} F_\lambda = nF_A \ ; \ B = \sum_{\lambda=3850\text{Å}}^{3950\text{Å}} F_\lambda = nF_B \ , \tag{A.8}$$

where n is the number of elements. We refer to the numerator in terms of A and B and their respective errors, σ_A and σ_B:

$$\left(\frac{\sigma_{\mathrm{D}_n}}{\mathrm{D}_n(4000)}\right)^2 = \left(\frac{\sqrt{n}\sigma_A}{nF_A}\right)^2 + \left(\frac{\sqrt{n}\sigma_B}{nF_B}\right)^2 \ . \tag{A.9}$$

Considering that $\sigma_A/F_A = \sigma_B/F_B = S/N$:

$$\left(\frac{\sigma_{\mathrm{D}_n}}{\mathrm{D}_n(4000)}\right)^2 = 2\left(\frac{1}{\sqrt{n}S/N}\right)^2 \ . \tag{A.10}$$

Isolating the S/N term we have:

$$S/N = \sqrt{\frac{2}{n}}\frac{\mathrm{D}_n(4000)}{\sigma_{\mathrm{D}_n}} \sim 2.8 \ , \tag{A.11}$$

where we consider a maximum value of $\mathrm{D}_n(4000) = 2$, $n = 100$ and a maximum value of error of $\sigma_{\mathrm{D}_n} = 0.1$.

Both spectral indices $H_{\delta,A}$ and $D_n(4000)$ are in a narrow region of the galaxy spectrum, allowing us to consider that the S/N of both spectral indices are approximately the same. Once the $H_{\delta,A}$ region has enough S/N to calculate this spectral index with a considerable error ($\sigma_{H_{\delta,a}} < 1.5$), the $D_n(4000)$ region will automatically have sufficient S/N to properly measure this index with an error of $\sigma_{\mathrm{D}_n} < 0.1$.